Chapter 6

Identification of novel multi-target N-benzyl piperazinyl sulfonamide derivatives for the management of AD

6.1 Introduction

Amyloid β, the major aggregatory component of amyloid plaques in the brain, is composed of heterogeneous peptides of 38–43 amino acids.The amino acids are excised from an integral membrane protein called amyloid precursor protein (APP) by the β- and γ-secretase enzymes. Aβ is the predominant aggregatory component of amyloid plaques in the brain, of which, $A\beta_{1-40}$ is the most prevalent version. Despite being less prevalent, $A\beta_{1-42}$ is thought to be harmful due to a greater propensity to form Aβ oligomers. It is released into extracellular spaces either directly into the interstitial fluids or synaptic clefts or through the secretory route. Aβ has been proposed to regulatethe synaptic plasticity at physiological levels [134].

Presenilin-1 and -2 (PS1 and PS2), components of the γ-secretase, along with APP could be affected by genetic mutations leading to an increased synthesis of $A\beta_{1-42}$ close to the lipid bilayer. The majority of famillial mutations in presenilin-1 or -2 shift the natural balance between $A\beta_{40}$ and $A\beta_{42/43}$ in favour of $A\beta_{42/43}$ production.

Since, BACE1 triggers the production of Aβ, its activity is predicted to be closely connected with the pathogenic processes that are mediated byAβ. Certainly, BACE1 levels are around two times higher in AD brains than in normal, non-demented brains [135].

In order to avoid or reverse Aβ-mediated impairments in AD patients, it makes sense to inhibit BACE1 activity. A more promising fact is that the abnormalities in BACE1-null mice are milder than those in animals with disrupted γ-secretase functioning. Targeted inhibition of BACE1 helps to lower the Aβ levels, in the past 20 years, it has been increasingly clear that a pathological amount of Aβ impairs synaptic processes.

BACE1 is a strcuturally complex protein that shares similarities with other aspartyl proteases, a family of enzymes that include BACE2, pepsin, renin, cathepsin D (CatD), and cathepsin E (CatE) found in various locations throughout the human body. Therefore, attaining selectivity in BACE1 inhibition without impacting other proteases is essential for the development of efficient BACE1 inhibitors to avoid off-target effects[136].

With the approval of Lecanemab (Leqembi), a recombinant humanized immunoglobulin gamma 1 (IgG1) monoclonal antibody and an inhibitor of soluble and insoluble forms of aggregated Aβ, there is a renewed interest in the discovery of agents targeting the Aβ pathology. Hence, the development of selective BACE-1 inhibitors with disease-modifying action reamins the need of the hour.

6.2 Materials and methods

6.2.1 Pharmacophore development and virtual screening

Pharmacophore models are indispensable tools in drug discovery, offering a systematic approach to ligand recognition and aiding in the identification and optimization of compounds with therapeutic potential. Themodels provide a conceptual framework that represents molecular features essential for recognizing a ligand by a biological macromolecule. It includes hydrophobic moieties, hydrogen bond donors, acceptors, aromatic rings, cations, and anions. These features can be present on the ligand or projected into the receptor. Pharmacophore models help identify chemical groups with similar properties, enabling the discovery of novel ligands. They are used in drug discovery in virtual screening, aiding in the identification of compounds with key features and potential binding affinity to the target macromolecule. Pharmacophore models also contribute significantly to hit identification from high-throughput screening data and the optimization of lead compounds. The deconstruction of pharmacophore models into human-interpretable maps streamlines hit and lead optimization efforts. Pharmacophore models play a pivotal role in scaffold hopping, identifying compounds with similar features but distinct scaffolds.

Hydrophobic features are crucial in pharmacophore models, which include hydrophobic volumes and hydrogen bond vectors. Hydrogen bond acceptor (HBA) and hydrogen bond donor (HBD) features are important descriptors used to define the pharmacophore. An HBA is an atom that can accept a hydrogen bond and are typically represented by blue spheres in

pharmacophore models. HBAs are important for ligand-receptor interactions as they form hydrogen bonds with the receptor. Similarly, an HBD is an atom that can donate a hydrogen bond and are typically represented by red spheres in pharmacophore models. HBDs are important for ligand-receptor interactions be-cause they can form hydrogen bonds with the receptor.

The Protein structure of BACE 1 protein was obtained from Protein Data Bank server (PDB id. 3KMY). Co-crystallized ligand 3-[2-(3-chlorophenyl) ethyl] pyridin-2-amine was used for the development of pharmacophore. Using the Pharmit server, the ZINC database of small molecular ligands was screened taking features from the resulting pharmacophore. The resultant compounds were then put through additional filters, including PAINS and Drug-likeness. Additionally, high-throughput virtual screening, standard precision docking, and extra precision docking were all applied to the compounds [137].

6.2.2 Molecular docking

6.2.2.1 Protein structure analysis

Chimera 1.13.1rc was used to carry out the structural analysis of the BACE 1 enzyme protein (PDB id. 3KMY) to identify any missing side chains and loops. Ramachandran plot of the protein showed zero groups in the disallowed region and an overall core part of 93.33%. The protein had an overall quality factor of 93.7023 with 86.02% of the residues having average 3D-1D score ≥ 0.1 [138].

6.2.2.2 Protein preparation

The model was refined using Discovery studio 2021. Ligands present in the complex were removed, hydrogen atoms were added, charges and pKa were given to amino acid residues using the PDB2PQR server at physiological pH of 7.4 and energy minimization of the protein was carried out. The protein was opened in Autodock tools 1.5.6, non-polar hydrogens were merged, and atom types were assigned. The pdb was finally stored as a pdbqt file.

6.2.2.3 Ligand preparation

Chemdraw structures of the ligands were saved in an sdf format. Chem 3D was used for energy minimization of the resulting structure. The steepest descent algorithm was employed for 4000 steps with the Generalised Amber Force Field (GAFF). The structures produced after minimization were imported into Autodock Tools 1.5.6 and converted to PDBQT format.

6.2.2.4 Grid generation

Grid maps of interaction energies with the various atom types present in the ligands (A, C, HD, NA, N, OA, S, Br, Cl, and I) were calculated by Autodock using autogrid 4.0. The prepared protein's grid size was set to 60X60X60 xyz points with a grid spacing of 0.375. The coordinates (x, y, and z) for the grid centre were 21.578, -6.531, and 32.509, respectively.

6.2.2.5 Docking

Autodock 4.0 was used to carry out the docking, Lamarckian Genetic Algorithm (LGA) was employed for the docking, with 10 runs, a 150 population size, a maximum of 2,500,000 energy evaluations, and a maximum of 27,000 generations. The calculated free binding energy of the ligand-receptor complex was employed in a semi-empirical free energy force field to score different conformations produced via molecular docking. Use of Discovery Studio 2021 allowed the visualization of docked conformers.

Whole molecule superposition was carried out using the superimposition tool in the Schrödinger Suite. The Superimposition tool was selected and reference and target structures defined. The tool then attempts to align the target structures onto the reference. Parameters like alignment method and weighting factors are adjusted based on the tool. The superimposition algorithm is executed to align structures based on criteria like minimizing the RMSD among the atoms. Results were analyzed to determine the alignment's effectiveness through visualization of the structures as well as extraction of RMSD data.

The conformation and binding of the piperazine ring can be influenced by the length and flexibility of the linker that connects it to the rest of molecule. Hydrogen bonding becomes an important aspect for binding of the piperazine moiety to the active site residues of AChE. The introduction of substituents that promote hydrogen bonding has the potential to increase the strength of binding interactions. The significance of steric factors of the substituents on piperazine ring or other molecular components may be noteworthy, particularly when the target enzyme exhibits distinct stereochemical preferences.

6.2.3 Chemistry

Sigma-Aldrich was used to acquire compounds 30 through 45 as well as 60-65. Thin layer chromatography (TLC) was employed to track the progress of the reactions on precoated silica gel 60 F254 plates (Merck KGaA), and ultraviolet light (254 nm) or iodine vapours were used to visualize the spots. In column chromatography, silica gel (60–120 mesh size) was utilised as an adsorbent to purify the compounds. Automated melting point apparatus (Bamstead Electrothermal, UK) was used to measure the melting points. On a Bruker Advance 500 MHz spectrometer, ^{1}H NMR and ^{13}C NMR spectra were captured in and $CDCl_3$, respectively. The coupling constant (J) was measured in Hz and the chemical shift was recorded in ppm (δ). Mass analysis was carried out on LC-MS Spectrometer Model Q-ToF Micro Waters.

General procedure for the synthesis of *(4-substituted) sulfonyl) 2-(4-hydroxyphenyl) aminoacetic acid* (45-60)

2-(4-hydroxyphenyl)aminoacetic acid (0.0073 moles, one equivalent) and sodium carbonate (0.0219 mol, three equivalent) were dissolved in a solution of 30 ml water and 10 ml acetone. The reaction mixture was then added with 20 mL of acetone and 0.0073 mol of variously substituted benzene sulfonyl chlorides and was stirred at room temperature (RT) for 24 hours. Ethyl acetate and hexane (4:6) mobile phase was used in TLC to track the development of the reaction. As soon as the reaction was over , acetone was evaporated under reduced pressure. It

was neutralised with 1 N HCl to get the crude product. The product was recrystallized with 20% ethanol. [79, 89].

General procedure for the synthesis of *4-substituted-N-(2-oxo-3-(4-phenylpiperazin-1-yl) propyl) benzenesulfonamide/4-substituted-N-(2-oxo-3-(4-benzylpiperazin-1-yl) propyl) benzenesulfonamide* (65-84)

The variously substituted sulfonamide compounds **45-60** (1 equivalent) were dissolved in 25 mL of N,N-Dimethylformamide (DMF) along with triethylamine (3 equivalents). The reaction mixture was treated with N′-ethylcarbodi-imide hydrochloride (EDC.HCl) (2.5 mM, 1.5 equivalent) and hydroxybenzotriazole (HOBt) (2.55 mM, 1.5 equivalent), followed by the addition of the appropriate piperazines (61-62) (1.1 equivalent). The reaction was monitored by TLC using ethyl acetate and methanol (8:2) as the mobile phase. After 6- to 8-hours of reflux, DMF was evaporated under reduced pressure. The resulting residue was extracted with ethyl acetate after washing with a saturated sodium bicarbonate solution. Ethyl acetate in hexane was usedas mobile phase in column chromatography over silica gel (60–120 mesh) to purify the product. The product was filtered and recrystallized with methanol to get the pure compound.

Step-1

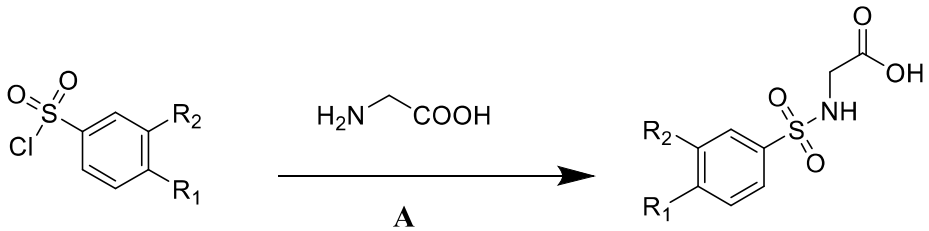

30C-44 **45-60**

Step-2

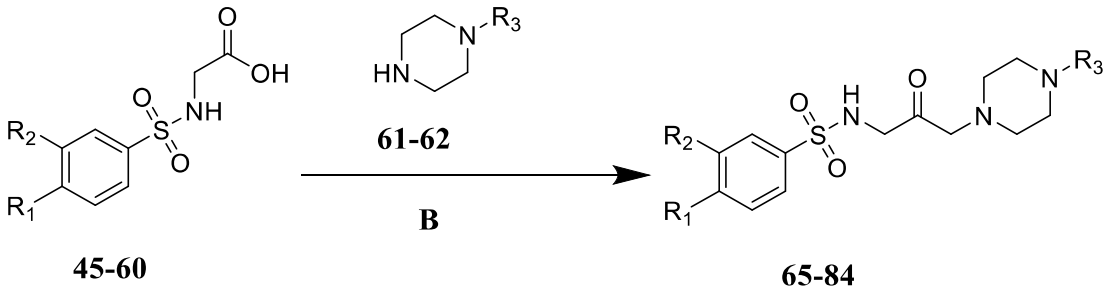

45-60 **65-84**

Reagents and conditions: **A**) Na_2CO_3/K_2CO_3, Water-Acetone mixture (1:1); RT, 24 hrs. **B**) TEA, DMF; Reflux,16 hrs.

(2-oxo-2-(4-phenylpiperazin-1-yl)ethyl)benzenesulfonamide (**65**): ^{1}H NMR (500 MHz, Chloroform) δ 7.92 – 7.80 (m, 2H, NH), 7.56 (s, 1H, ArH), 7.49 – 7.43 (m, 2H, ArH), 7.13 – 7.06 (m, 2H, ArH), 6.66 – 6.59 (m, 3H, ArH), 4.38 (s, 1H), 4.18 (s, 1H, CH_2), 3.88 (s, 1H, piperazin-CH_2), 3.82 – 3.78 (m, 2H, piperazin-CH_2), 3.70 – 3.66 (m, 2H, piperazin-CH_2), 3.59 – 3.55 (m, 2H, piperazin-CH_2), 3.47 – 3.43 (m, 2H, piperazin-CH_2). ^{13}C NMR (125 MHz, Chloroform) δ 167.43 (s), 150.96 (s), 139.59 (s), 133.95 (s), 129.54 – 129.14 (m), 129.08 – 128.87 (m), 128.17 – 127.95 (m), 120.31 (s), 116.88 – 116.66 (m), 49.91 – 49.70 (m), 45.03 – 44.64 (m), 44.27 (s). MS (ESI): *m/z* found 360.17 [M^+]; calculated for $C_{18}H_{21}N_3O_3S$ 359.13

4-chloro-N-(2-oxo-2-(4-phenylpiperazin-1-yl)ethyl)benzenesulfonamide (**66**): ^{1}H NMR (500 MHz, Chloroform) δ 7.99 – 7.84 (m, 2H, NH), 7.58 – 7.44 (m, 2H, ArH), 7.12 – 7.07 (m, 2H, ArH), 6.70 – 6.52 (m, 3H, ArH), 6.14 (s, 1H), 4.33 (s, 1H), 4.16 (s, 1H, CH_2), 3.82 – 3.78 (m, 2H, piperazin-CH_2), 3.70 – 3.66 (m, 2H, piperazin-CH_2), 3.60 – 3.56 (m, 2H, piperazin-CH_2), 3.47 – 3.43 (m, 2H, piperazin-CH_2).). ^{13}C NMR (125 MHz, Chloroform) δ 167.43 (s), 150.96 (s), 141.43 (s), 140.47 (s), 129.64 – 129.43 (m), 129.43 – 129.14 (m), 120.31 (s), 116.88 – 116.66 (m), 49.91 – 49.70 (m), 45.03 – 44.64 (m), 44.27 (s). MS (ESI): *m/z* found 394.09 [M^+], 396.17; calculated for $C_{18}H_{20}ClN_3O_3S$ 393.09

4-bromo-N-(2-oxo-2-(4-phenylpiperazin-1-yl)ethyl)benzenesulfonamide (**67**): ^{1}H NMR (500 MHz, Chloroform) δ 7.90 – 7.76 (m, 2H, NH), 7.76 – 7.62 (m, 2H, ArH), 7.12 – 7.06 (m, 2H,

ArH), 6.71 – 6.58 (m, 3H, ArH), 5.88 (s, 1H), 4.32 (s, 1H, CH_2), 3.84 – 3.78 (m, 3H, piperazin-CH_2), 3.75 – 3.71 (m, 2H, piperazin-CH_2), 3.59 – 3.55 (m, 2H, piperazin-CH_2), 3.49 – 3.45 (m, 2H, piperazin-CH_2). ^{13}C NMR (125 MHz, Chloroform) δ 167.43 (s), 150.96 (s), 138.86 (s), 132.18 – 131.97 (m), 130.07 (s), 129.82 – 129.43 (m), 129.43 – 129.14 (m), 120.31 (s), 116.88 – 116.66 (m), 49.91 – 49.70 (m), 45.03 – 44.64 (m), 44.27 (s). MS (ESI): *m/z* found 438.05 [M^+], 440.52; calculated for $C_{18}H_{20}BrN_3O_3S$ 437.04

4-nitro-N-(2-oxo-2-(4-phenylpiperazin-1-yl)ethyl)benzenesulfonamide (**68**): ^{1}H NMR (500 MHz, Chloroform) δ 8.48 – 8.34 (m, 2H, ArH), 8.28 – 8.14 (m, 2H, NH), 7.14 – 7.10 (m, 2H, ArH), 6.76 – 6.66 (m, 3H, ArH), 5.96 (s, 1H), 4.29 (s, 1H), 4.10 (s, 1H, CH_2), 3.86 – 3.82 (m, 2H, piperazin-CH_2), 3.74 – 3.70 (m, 2H, piperazin-CH_2), 3.64 – 3.60 (m, 2H, piperazin-CH_2), 3.53 – 3.49 (m, 2H, piperazin-CH_2). ^{13}C NMR (125 MHz, Chloroform) δ 167.43 (s), 150.96 (s), 150.10 (s), 142.50 (s), 129.54 – 129.21 (m), 122.94 – 122.73 (m), 120.31 (s), 116.88 – 116.66 (m), 49.91 – 49.70 (m), 45.03 – 44.64 (m), 44.27 (s). MS (ESI): *m/z* found 405.12 [M^+]; calculated for $C_{18}H_{20}N_4O_5S$ 404.12

2-nitro-N-(2-oxo-2-(4-phenylpiperazin-1-yl)ethyl)benzenesulfonamide (**69**): ^{1}H NMR (500 MHz, Chloroform) δ 8.20 (d, J = 2.9 Hz, 2H, ArH), 7.83 (d, J = 13.4 Hz, 2H, NH), 7.12 – 7.05 (m, 2H, ArH), 6.68 – 6.53 (m, 3H, ArH), 4.33 (d, J = 19.2 Hz, 2H), 3.91 (s, 1H, CH_2), 3.81 – 3.77 (m, 2H, piperazin-CH_2), 3.71 – 3.67 (m, 2H, piperazin-CH_2), 3.67 – 3.63 (m, 2H, piperazin-CH_2), 3.47 – 3.43 (m, 2H, piperazin-CH_2). ^{13}C NMR (125 MHz, Chloroform) δ 167.43 (s), 151.73 (s), 150.96 (s), 136.53 (s), 134.90 (s), 132.64 (s), 129.54 – 129.14 (m), 128.26 (s), 126.12 (s), 120.31 (s), 116.88 – 116.66 (m), 49.91 – 49.70 (m), 45.03 – 44.64 (m), 44.27 (s). MS (ESI): *m/z* found 405.12 [M^+]; calculated for $C_{18}H_{20}N_4O_5S$ 404.12

4-methoxy-N-(2-oxo-2-(4-phenylpiperazin-1-yl)ethyl)benzenesulfonamide (**70**): ^{1}H NMR (500 MHz, Chloroform) δ 7.98 – 7.84 (m, 2H, NH), 7.20 – 7.06 (m, 4H, ArH), 6.71 – 6.58 (m, 3H, ArH), 4.87 (s, 1H), 4.28 (s, 1H), 4.15 (s, 1H, CH_2), 3.83 – 3.79 (m, 5H, CH_3), 3.78 – 3.74 (m,

2H, piperazin-CH_2), 3.58 – 3.54 (m, 2H, piperazin-CH_2), 3.49 – 3.45 (m, 2H, piperazin-CH_2). ^{13}C NMR (125 MHz, Chloroform) δ 167.43 (s), 162.79 (s), 150.96 (s), 132.28 (s), 129.59 – 129.14 (m), 120.31 (s), 116.88 – 116.66 (m), 112.99 – 112.60 (m), 56.04 (s), 49.91 – 49.70 (m), 45.03 – 44.64 (m), 44.27 (s). MS (ESI): *m/z* found 390.15 [M^+]; calculated for $C_{19}H_{23}N_3O_4S$ 389.14

4-cyano-N-(2-oxo-2-(4-phenylpiperazin-1-yl)ethyl)benzenesulfonamide (**71**): ^{1}H NMR (500 MHz, Chloroform) δ 8.19 – 8.04 (m, 2H, ArH), 7.91 – 7.76 (m, 2H, ArH), 7.14 – 7.09 (m, 2H, ArH), 6.75 – 6.66 (m, 3H), 5.33 (s, 1H), 4.39 (s, 1H), 4.20 (s, 1H, CH_2), 3.82 – 3.78 (m, 2H, piperazin-CH_2), 3.76 – 3.72 (m, 2H, piperazin-CH_2), 3.67 – 3.63 (m, 2H, piperazin-CH_2), 3.51 – 3.47 (m, 2H, piperazin-CH_2). ^{13}C NMR (125 MHz, Chloroform) δ 167.43 (s), 150.96 (s), 148.23 (s), 133.76 – 133.55 (m), 129.70 – 129.49 (m), 129.49 – 129.14 (m), 120.31 (s), 119.36 (s), 119.12 (s), 116.88 – 116.66 (m), 49.91 – 49.70 (m), 45.03 – 44.64 (m), 44.27 (s). MS (ESI): *m/z* found 385.13 [M^+]; calculated for $C_{19}H_{20}N_4O_3S$ 384.13

N-(2-oxo-2-(4-phenylpiperazin-1-yl)ethyl)-[1,1'-biphenyl]-4-sulfonamide (**72**): ^{1}H NMR (500 MHz, Chloroform) δ 8.19 – 8.04 (m, 2H, ArH), 7.93 – 7.78 (m, 2H, ArH), 7.69 – 7.56 (m, 2H, ArH), 7.49 – 7.43 (m, 2H, ArH), 7.38 (s, 1H, NH), 7.14 – 7.08 (m, 2H, ArH), 6.74 – 6.64 (m, 3H, ArH), 5.30 (s, 1H), 4.40 (s, 1H), 4.21 (s, 1H, CH_2), 3.83 – 3.79 (m, 2H, piperazin-CH_2), 3.77 – 3.73 (m, 2H, piperazin-CH_2), 3.68 – 3.64 (m, 2H, piperazin-CH_2), 3.51 – 3.47 (m, 2H, piperazin-CH_2). ^{13}C NMR (125 MHz, Chloroform) δ 167.43 (s), 150.96 (s), 148.49 (s), 145.70 (s), 140.41 (s), 129.85 – 129.46 (m), 129.46 – 129.14 (m), 129.02 – 128.81 (m), 128.66 – 128.13 (m), 127.40 – 127.18 (m), 120.31 (s), 116.88 – 116.66 (m), 49.91 – 49.70 (m), 45.03 – 44.64 (m), 44.27 (s). MS (ESI): *m/z* found 436.17 [M^+]; calculated for $C_{24}H_{25}N_3O_3S$ 435.16

N-(2-oxo-2-(4-phenylpiperazin-1-yl)ethyl)naphthalene-1-sulfonamide (**73**): ^{1}H NMR (500 MHz, Chloroform) δ 8.17 (d, J = 18.1 Hz, 5H, naphthalene-CH), 8.07 (s, 1H, naphthalene-CH), 7.84 (s, 2H, NH), 7.70 (s, 2H, naphthalene-CH), 7.50 (d, J = 16.3 Hz, 4H, naphthalene-CH),

7.10 – 7.04 (m, 4H, ArH), 6.69 – 6.59 (m, 6H, ArH), 5.71 (s, 2H), 4.29 (s, 2H), 4.03 (s, 2H, CH_2), 3.81 – 3.77 (m, 4H, piperazin-CH_2), 3.75 – 3.71 (m, 4H, piperazin-CH_2), 3.54 – 3.50 (m, 4H, piperazin-CH_2), 3.48 – 3.44 (m, 4H, piperazin-CH_2). ^{13}C NMR (125 MHz, Chloroform) δ 167.43 (s), 150.96 (s), 134.71 (s), 134.14 – 133.56 (m), 131.49 (d, J = 3.1 Hz), 129.54 – 129.14 (m), 127.77 (s), 126.85 (s), 123.86 (s), 122.19 (s), 120.31 (s), 116.88 – 116.66 (m), 49.91 – 49.70 (m), 45.03 – 44.64 (m), 44.27 (s). MS (ESI): *m/z* found 410.15 [M^+]; calculated for $C_{22}H_{23}N_3O_3S$ 409.15

4-(sec-butyl)-N-(2-oxo-2-(4-phenylpiperazin-1-yl)ethyl)benzenesulfonamide (**74**): ^{1}H NMR (500 MHz, Chloroform) δ 8.00 – 7.86 (m, 2H, ArH), 7.58 – 7.44 (m, 2H, ArH), 7.14 – 7.08 (m, 2H, ArH), 6.75 – 6.65 (m, 3H, ArH), 5.24 (s, 1H), 4.39 (s, 1H), 4.20 (s, 1H, CH_2), 3.82 – 3.78 (m, 2H, piperazin-CH_2), 3.76 – 3.72 (m, 2H, piperazin-CH_2), 3.68 – 3.64 (m, 2H, piperazin-CH_2), 3.50 – 3.46 (m, 2H, piperazin-CH_2), 2.97 (s, 1H, *sec-butyl-CH*), 1.65 (d, J = 5.7 Hz, 2H, *sec-butyl-* CH_2), 1.42 – 1.28 (m, 3H), 1.01 – 0.97 (m, 3H). ^{13}C NMR (125 MHz, Chloroform) δ 167.43 (s), 154.06 (s), 150.96 (s), 138.85 (s), 129.54 – 129.14 (m), 128.34 – 128.13 (m), 127.21 – 126.81 (m), 120.31 (s), 116.88 – 116.66 (m), 49.91 – 49.70 (m), 45.03 – 44.64 (m), 44.27 (s), 41.17 (s), 29.08 (s), 20.12 (s), 10.88 (s). MS (ESI): *m/z* found 416.21 [M^+]; calculated for $C_{22}H_{29}N_3O_3S$ 415.19

N-(2-(4-benzylpiperazin-1-yl)-2-oxoethyl)benzenesulfonamide (**75**): ^{1}H NMR (500 MHz, Chloroform) δ 7.91 – 7.79 (m, 2H, ArH), 7.57 (s, 1H, NH), 7.51 – 7.45 (m, 2H, ArH), 7.32 – 7.24 (m, 4H, ArH), 7.22 (s, 1H), 4.35 (s, 1H), 4.25 (s, 1H), 4.09 (s, 1H, CH_2), 3.69 – 3.63 (m, 4H, CH_2), 3.40 – 3.36 (m, 2H, piperazin-CH_2), 2.88 – 2.84 (m, 2H, piperazin-CH_2), 2.66 – 2.62 (m, 2H, piperazin-CH_2). ^{13}C NMR (125 MHz, Chloroform) δ 167.43 (s), 139.59 (s), 138.23 (s), 133.95 (s), 129.08 – 128.88 (m), 128.88 – 128.70 (m), 128.17 – 127.75 (m), 126.55 (s), 63.66 (s), 51.25 – 51.04 (m), 44.26 (t, J = 1.1 Hz). MS (ESI): *m/z* found 374.14 [M^+]; calculated for $C_{19}H_{23}N_3O_3S$ 373.15

N-(2-(4-benzylpiperazin-1-yl)-2-oxoethyl)-4-chlorobenzenesulfonamide (**76**): ^{1}H NMR (500 MHz, Chloroform) δ 7.95 – 7.80 (m, 2H, NH), 7.59 – 7.45 (m, 2H, ArH), 7.33 – 7.21 (m, 5H, ArH), 4.46 (s, 1H), 4.37 (s, 1H), 4.09 (s, 1H, CH_2), 3.77 – 3.73 (m, 2H, piperazin-CH_2), 3.63 – 3.59 (m, 2H, CH_2), 3.40 – 3.36 (m, 2H, piperazin-CH_2), 2.92 – 2.85 (m, 4H, piperazin-CH_2). ^{13}C NMR (125 MHz, Chloroform) δ 167.43 (s), 141.43 (s), 140.47 (s), 138.23 (s), 129.64 – 129.43 (m), 129.43 – 129.27 (m), 128.92 – 128.70 (m), 128.14 – 127.75 (m), 126.55 (s), 63.66 (s), 51.25 – 51.04 (m), 44.26 (t, J = 1.1 Hz). MS (ESI): *m/z* found 408.12[M^+], 410.32; calculated for $C_{19}H_{22}ClN_3O_3S$ 407.11

N-(2-(4-benzylpiperazin-1-yl)-2-oxoethyl)-4-bromobenzenesulfonamide (**77**): ^{1}H NMR (500 MHz, Chloroform) δ 7.91 – 7.76 (m, 2H, ArH), 7.76 – 7.62 (m, 2H, ArH), 7.33 – 7.21 (m, 5H, ArH), 4.44 (s, 1H), 4.31 (s, 1H), 4.12 (s, 1H, CH_2), 3.80 – 3.76 (m, 2H, piperazin-CH_2), 3.67 – 3.63 (m, 2H, CH_2), 3.39 – 3.35 (m, 2H, piperazin-CH_2), 2.85 – 2.79 (m, 4H, piperazin-CH_2). ^{13}C NMR (125 MHz, Chloroform) δ 167.43 (s), 138.86 (s), 138.23 (s), 132.18 – 131.97 (m), 130.07 (s), 129.82 – 129.43 (m), 128.92 – 128.70 (m), 128.14 – 127.75 (m), 126.55 (s), 63.66 (s), 51.25 – 51.04 (m), 44.26 (t, J = 1.1 Hz). MS (ESI): *m/z* found 452.06[M^+], 454.47; calculated for $C_{19}H_{22}BrN_3O_3S$ 451.06

N-(2-(4-benzylpiperazin-1-yl)-2-oxoethyl)-[1,1'-biphenyl]-4-sulfonamide (**78**): ^{1}H NMR (500 MHz, Chloroform) δ 8.17 – 8.03 (m, 2H, ArH), 7.89 – 7.75 (m, 2H, NH), 7.64 – 7.51 (m, 2H, ArH), 7.48 – 7.42 (m, 2H, ArH), 7.37 (s, 1H), 7.32 – 7.25 (m, 4H, ArH), 7.22 (s, 1H), 5.80 (s, 1H), 4.21 (s, 1H), 4.12 (s, 1H, CH_2), 3.70 – 3.66 (m, 2H, CH_2), 3.60 – 3.56 (m, 2H, piperazin-CH_2), 3.40 – 3.36 (m, 2H, piperazin-CH_2), 2.87 – 2.83 (m, 2H, piperazin-CH_2), 2.67 – 2.63 (m, 2H, piperazin-CH_2). ^{13}C NMR (125 MHz, Chloroform) δ 167.43 (s), 148.49 (s), 145.70 (s), 140.41 (s), 138.23 (s), 129.85 – 129.46 (m), 129.02 – 128.70 (m), 128.66 – 128.14 (m), 128.14 – 127.75 (m), 127.40 – 127.18 (m), 126.55 (s), 63.66 (s), 51.25 – 51.04 (m), 44.26 (t, J = 1.1 Hz). MS (ESI): *m/z* found 450.17 [M^+]; calculated for $C_{25}H_{27}N_3O_3S$ 449.18

N-(2-(4-benzylpiperazin-1-yl)-2-oxoethyl)-2-nitrobenzenesulfonamide (**79**): ^{1}H NMR (500 MHz, Chloroform) δ 8.28 (d, J = 2.5 Hz, 2H, ArH), 7.91 (s, 1H, NH), 7.87 (s, 1H), 7.31 – 7.19 (m, 5H, ArH), 6.49 (s, 1H), 4.25 (s, 1H), 4.01 (s, 1H, CH_2), 3.69 – 3.65 (m, 2H, CH_2), 3.63 – 3.59 (m, 2H, piperazin-CH_2), 3.42 – 3.38 (m, 2H, piperazin-CH_2), 2.87 – 2.83 (m, 2H, piperazin-CH_2), 2.74 – 2.70 (m, 2H, piperazin-CH_2). ^{13}C NMR (125 MHz, Chloroform) δ 167.43 (s), 151.73 (s), 138.23 (s), 136.53 (s), 134.90 (s), 132.64 (s), 128.92 – 128.70 (m), 128.26 (s), 128.14 – 127.75 (m), 126.55 (s), 126.12 (s), 63.66 (s), 51.25 – 51.04 (m), 44.46 – 44.14 (m). MS (ESI): *m/z* found 419.13 [M^+]; calculated for $C_{19}H_{22}N_4O_5S$ 418.13

N-(2-(4-benzylpiperazin-1-yl)-2-oxoethyl)-4-nitrobenzenesulfonamide (**80**): ^{1}H NMR (500 MHz, Chloroform) δ 8.47 – 8.33 (m, 2H, NH), 8.27 – 8.13 (m, 2H, ArH), 7.33 – 7.21 (m, 5H, ArH), 5.93 (s, 1H), 4.26 (s, 1H), 4.09 (s, 1H, CH_2), 3.70 – 3.66 (m, 2H, CH_2), 3.61 – 3.57 (m, 2H, piperazin-CH_2), 3.41 – 3.37 (m, 2H, piperazin-CH_2), 2.89 – 2.85 (m, 2H, piperazin-CH_2), 2.68 – 2.64 (m, 2H, piperazin-CH_2). ^{13}C NMR (125 MHz, Chloroform) δ 167.43 (s), 150.10 (s), 142.50 (s), 138.23 (s), 129.52 – 129.12 (m), 128.92 – 128.70 (m), 128.14 – 127.75 (m), 126.55 (s), 122.94 – 122.73 (m), 63.66 (s), 51.25 – 51.04 (m), 44.26 (t, J = 1.1 Hz). MS (ESI): *m/z* found 419.13 [M^+]; calculated for $C_{19}H_{22}N_4O_5S$ 418.13

N-(2-(4-benzylpiperazin-1-yl)-2-oxoethyl)-4-cyanobenzenesulfonamide (**81**): ^{1}H NMR (500 MHz, Chloroform) δ 8.20 – 8.06 (m, 2H, ArH), 7.91 – 7.77 (m, 2H, NH), 7.34 – 7.17 (m, 5H, ArH), 4.43 (s, 1H), 4.16 (s, 1H), 4.11 (s, 1H, CH_2), 3.56 – 3.50 (m, 4H, CH_2), 3.24 – 3.20 (m, 2H, piperazin-CH_2), 2.90 – 2.86 (m, 2H, piperazin-CH_2), 2.85 – 2.81 (m, 2H, piperazin-CH_2). ^{13}C NMR (125 MHz, Chloroform) δ 167.43 (s), 148.23 (s), 138.23 (s), 133.76 – 133.55 (m), 129.70 – 129.49 (m), 128.92 – 128.70 (m), 128.14 – 127.75 (m), 126.55 (s), 119.36 (s), 119.12 (s), 63.66 (s), 51.25 – 51.04 (m), 44.26 (t, J = 1.1 Hz). MS (ESI): *m/z* found 399.15 [M^+]; calculated for $C_{20}H_{22}N_4O_3S$ 398.14

N-(2-(4-benzylpiperazin-1-yl)-2-oxoethyl)-4-methoxybenzenesulfonamide (**82**): ^{1}H NMR (500 MHz, Chloroform) δ 8.07 – 7.93 (m, 2H, NH), 7.31 – 7.26 (m, 1H, ArH), 7.26 – 7.17 (m, 6H, ArH), 4.60 (s, 1H), 4.37 (s, 1H), 4.23 (s, 1H), 4.04 – 4.00 (m, 2H, CH_2), 3.82 – 3.78 (m, 3H, CH_3), 3.36 – 3.32 (m, 2H, piperazin-CH_2), 3.26 – 3.22 (m, 2H, piperazin-CH_2), 3.05 – 3.01 (m, 2H), 2.67 – 2.63 (m, 2H, piperazin-CH_2). ^{13}C NMR (125 MHz, Chloroform) δ 167.43 (s), 162.79 (s), 138.23 (s), 132.28 (s), 129.59 – 129.38 (m), 128.92 – 128.70 (m), 128.14 – 127.75 (m), 126.55 (s), 112.99 – 112.60 (m), 63.66 (s), 56.04 (s), 51.25 – 51.04 (m), 44.26 (t, J = 1.1 Hz). MS (ESI): *m/z* found 404.16 [M^+]; calculated for $C_{20}H_{25}N_3O_4S$ 403.16

N-(2-(4-benzylpiperazin-1-yl)-2-oxoethyl)-4-(sec-butyl)benzenesulfonamide (**83**): ^{1}H NMR (500 MHz, Chloroform) δ 7.99 – 7.85 (m, 2H, ArH), 7.59 – 7.45 (m, 2H, ArH), 7.33 – 7.24 (m, 4H, ArH), 7.22 (s, 1H, NH), 4.22 (s, 1H), 4.11 (s, 1H, CH_2), 3.96 (s, 1H), 3.68 – 3.64 (m, 2H, CH_2), 3.59 – 3.55 (m, 2H, piperazin-CH_2), 3.39 – 3.35 (m, 2H, piperazin-CH_2), 2.84 (t, J = 3.7 Hz, 3H), 2.66 – 2.62 (m, 2H, sec-butyl- CH_2), 1.65 (s, 1H), 1.57 (s, 1H), 1.42 – 1.28 (m, 3H, sec-butyl- CH_2), 1.02 – 0.98 (m, 3H, sec-butyl- CH_3). ^{13}C NMR (125 MHz, Chloroform) δ 167.43 (s), 154.06 (s), 138.85 (s), 138.23 (s), 128.92 – 128.70 (m), 128.34 – 128.14 (m), 128.14 – 127.75 (m), 127.21 – 126.81 (m), 126.55 (s), 63.66 (s), 51.25 – 51.04 (m), 44.26 (t, J = 1.1 Hz), 41.17 (s), 29.08 (s), 20.12 (s), 10.88 (s). MS (ESI): *m/z* found 430.22 [M^+]; calculated for $C_{23}H_{31}N_3O_3S$ 429.21

N-(2-(4-benzylpiperazin-1-yl)-2-oxoethyl)naphthalene-2-sulfonamide (**84**): ^{1}H NMR (500 MHz, Chloroform) δ 8.39 (s, 1H, naphthalene-CH), 8.06 (d, J = 30.7 Hz, 2H, naphthalene-CH), 7.86 (d, J = 17.3 Hz, 2H, NH), 7.49 (d, J = 3.7 Hz, 2H, naphthalene-CH), 7.30 – 7.18 (m, 5H, ArH), 6.07 (s, 1H), 4.30 (s, 1H), 4.07 (s, 1H, CH_2), 3.60 – 3.56 (m, 2H, CH_2), 3.42 – 3.35 (m, 4H, piperazin-CH_2), 2.84 – 2.80 (m, 2H, piperazin-CH_2), 2.66 – 2.62 (m, 2H, piperazin-CH_2). ^{13}C NMR (125 MHz, Chloroform) δ 167.43 (s), 142.68 (s), 138.23 (s), 134.09 (s), 133.66 (s), 131.56 (s), 130.35 (s), 129.11 (s), 128.92 – 128.70 (m), 128.53 (s), 128.14 – 127.75 (m), 126.96

(s), 126.52 (d, J = 6.6 Hz), 125.92 (s), 63.66 (s), 51.25 – 51.04 (m), 44.46 – 44.14 (m). MS (ESI): *m/z* found 424.17 [M^+]; calculated for $C_{23}H_{25}N_3O_3S$ 423.16

6.2.4 Biology

6.2.4.1 In-vitro AChE and BChE inhibition assays

Chapter 4 section 4.2.5.1of the thesis includes a detailed procedure of assay. Seven different concentrations (0.1-1000 nM) of test compounds were used in the enzyme inhibition studies.

6.2.4.2 In-vitro BACE-1 inhibition assay

BACE-1 activity was determined by using a β-secretase (BACE-1) activity detection kit, which included 7-methoxycoumarin-4-acetyl- [Asn^{670}, Leu^{671}]-amyloid β/A4 precursor protein 770 fragment 667-676-(2,4-dinitrophenyl) Lys-Arg-Arg trifluoroacetate amide salt as the substrate. Stock solution of the substrate (1mg/ml) (500 μM) was prepared by adding 0.5 ml of DMSO to the BACE-1 solution and stored. Prior to the commencement of the assay, an aliquot of the stock solution was diluted to 50 μM strength using the fluorescent assay buffer. The 96 well fluorometer plate was prepared as per the protocol furnished by the manufacturer. addition of the BACE-1 enzyme was immediately followed by the was measurement of fluorescence intensity with excitation and emission wavelengths set at 320 nm and 405 nm, respectively.

Different inhibitor doses capable of inhibiting the enzyme were taken in the range of 20 and 80. Covered plates were incubated for 2 hours at 37 °C and fluorescence intensity was again measured using a Multimode Microplate Reader (BioTek Synergy H1M, USA). The experiments were conducted in duplicate and were carried out twice. The expression: [(IFo-IFi)/IFo] 100. [(IFo–IFi)/IFo] × 100, was used to calculate the percentage inhibitions, where IFi and IFo are the fluorescence intensities obtained in the presence and absence of the inhibitor, respectively. The IC_{50} values were calculated using linear regression graph (GraphPad Prism 5.1, GraphPad Software Inc.).

6.2.4.3 Thioflavin T assay

Aβ-redox active metals create ROS species causing neuronal death. Metal ions along with AChE were found to induce the aggregation of Aβ [82]. Thioflavin T (ThT) test was used to assess the inhibition potential of compounds against Fe^{+2} induced $A\beta_{1-42}$ aggregation [83]. Compounds were dissolved in DMSO and diluted with PBS while $A\beta_{1-42}$ (Sigma) was dissolved in phosphate buffer (PBS, 10 mM, pH 7.5). The ratio used to screen the synthesised compounds was 1:2 for $A\beta_{1-42}$: inhibitor. The selected compounds were then evaluated at various ratios of the $A\beta_{1-42}$: inhibitor (1:0.5, 1:1, 1:2). Both $A\beta_{1-42}$ and the compounds, had final concentration of 10 μM (2μL), 0.5, 10, 20 μM (2μL) and 10 μM (16 μL), respectively of Fe^{+2}. The mixtures were incubated at room temperature for 48h in dark. The fluorescence intensities of the incubated mixtures were measured at the end of experiment by adding 178 μL of 20 μM ThT at excitation and emission wavelengths of 485 and 528 nm respectively.

6.2.4.4 Confocal fluorescence imaging

The assay mentioned in section 6.3.2 was further used for the confocal fluorescence imaging. Using DABCO (Sigma, CAS-280-57-9) as the fixing agent, Fluorescence dye ThT; $A\beta_{1-42}$ and ThT; $A\beta_{1-42}$; $A\beta_{1-42}$ and $FeCl_3$; $A\beta_{1-42}$, $FeCl_3$ and ThT; $A\beta_{1-42}$, $FeCl_3$, compound **72** and ThT; compound **72** and ThT; compound **72** were incubated and mounted on a glass slide. All the Confocal imaging experiments were done at 10 and 20 mM of compound **72** [84].

6.2.4.5 Neurotoxicity assay

A neural induction medium (NIM) made up of minimal essential medium (MEM), 5% fetal bovine serum (FBS), and 10 μM retinoic acid (RA) was used to develop the neuronal cells (SH-SY5Y). After six days of cell growth in the NIM medium, the cells were transferred to the serum-free NIM media. On day 7, differentiated SH-SY5Y cells were used to test the cytotoxic potential of the compound 72 using the 3-(4,5- dimethylthiazol-2-yl)-2,5-diphenyltetrazolium bromide (MTT) assay. In 96-well plates, cells (1×103 cells/well) were seeded. Different

concentrations (15,30, and 60 µM) of the compound 72 as well as donepezil were added and then incubated for another 24 hours at 37 °C after the culture medium had been removed. No significant changes were observed with respect to the cell viability of the control as well as the treated cells even at a high dose of 80 µM. Additionally, each well received 20 µL of MTT solution (0.5 mg/mL), the plate was then incubated for 4 hours at 37 °C. After 4 hours, the medium was removed, 200 µL of DMSO was added, formazan crystal formation was detected, and absorbance at 570 nm was measured.

6.2.4.6 Neuroprotection assay

The assay protocol used in chapter 4 section 4.2.5.8 was used for the neuroprotection study. The study was performed in triplicate.

6.2.4.7 In-vitro blood-brain barrier permeation assay (PAMPA)

Parallel artificial membrane permeation assay (PAMPA-BBB) was used to test the permeability of the chosen drugs across the blood-brain barrier (BBB)**[139]**. Dodecane was bought from Avra Synthesis in Hyderabad, while porcine brain lipid (PBL) was supplied from Avanti Polar Lipids in Alabaster. Acceptor microplates with PVDF membrane, pore size 0.45 µm along with donor microplates were procured from Merck Millipore. 4 µL of 20 mg/ml PBL in dodecane was used to coat the acceptor plate subsequent to which, 200 µL of buffer (pH 7.4) was added. Compounds **65** through **84** were dissolved in 1 ml of DMSO at a concentration of 5 mg each. From there, 10 µL of each solution was collected and diluted 200-fold using a buffer of pH of 7.5, resulting in a final concentration of 25 µg/ml. The donor well plate received 200 µL of the compounds at a concentration of 25 µg/ml. The donor plate was placed carefully over the acceptor plate in a sandwiched manner and incubated for 18 hours. With the use of a microplate reader and its UV spectroscopy tools (HTX multi-mode reader, BioTek, USA), the drug concentration in the acceptor, donor, and reference wells were all determined. Each sample was scanned in three separate runs for at least five distinct wavelengths. The PAMPA

model was validated by using 9 (Verapamil, Diazepam, Progesterone, Atenolol, Dopamine, Lomefloxacin, Alprazolam, Chlorpromazine and Oxazepam) commercially available drugs of known BBB permeability [140].

6.2.4.8 Scopolamine induced amnesia model

6.2.4.8.1 Animals

Wistar rats (200− 250 g) of either sex were procured from Central Animal Facility, IMS (BHU), Varanasi, India. Animals were housed in polyacrylic cages with free access to commercial food and water. The temperature and relative humidity were kept under controlled conditions (25±2 °C and 55±10%, respectively) while housed in a 12 h light/dark cycle. The central animal ethical committee of the institute duly authorized the experiment procedures, which were carried out in accordance with CPCSEA standards (No. Dean/2022/CEC/93).

6.2.4.8.2 Acute Oral Toxicity Study

In order to calculate the LD_{50} of compound **72** at fixed dosages of 5, 50, and 300 mg/kg, the OECD guidelines were used. For each dose, three female Wistar rats were used. The three animal groups, each of which contained three female rats, received doses of 5, 50, and 300 mg/kg, and they were observed for 72 hours.

6.2.4.8.3 Administration of scopolamine

Scopolamine hydrobromide (3mg/kg) was dissolved in distilled water and administered i.p on the seventh day, 1 h after test or donepezil administration. The behavioral study was performed 5 min after scopolamine injection[141].

6.2.4.8.4 Experimental protocol and drug administration

The animals were divided into ten groups of nine animals each. Prior to administration, compound **72** and donepezil, were freshlysuspended in 0.3 % CMC. The following nine experimental groups of nine animals each were created: (i) vehicle control (0.3 % CMC) (ii)

Scopolamine (3 mg/kg); (iii) Scopolamine plus donepezil (3 mg/kg); (iv) Scopolamine plus Compound **72** (5 mg/kg); (v) Scopolamine plus Compound **72** (10 mg/kg); (vi) Scopolamine plus Compound **72** (20 mg/kg); (vii) Compound **72** (20 mg/kg). The dose of the substances were established based on their LD_{50}. All groups received their medications via intraperitoneal injection (i.p.). In various groups, donepezil and the test compound at various doses were given once daily for seven days. On the seventh day, scopolamine was given to all the group animals, excluding the vehicle control, to cause amnesia.

6.2.4.8.5 Evaluation of memory function: Y-Maze Test

All animals, other than the control group, received an intraperitoneal injection of scopolamine hydrobromide (0.5 mg/kg) on the seventh day of the trial, 30 minutes after the treatment. A five-minute scopolamine infusion was followed by a three-arm Y-maze test to assess immediate spatial working memory. The arms were cleaned thoroughly, with 70% v/v ethanol, and given the designations A, B, and C arms. Each rat was given its own spot in the maze's center. Rats were initially always inserted into the arm of facing, therefore the first entry was left out of the calculation. For a total of 8 minutes, the spontaneous alternation behaviour, the number of entries to all arms, and the number of entries to each arm were all recorded. Between each session, the maze was cleaned and wiped down. Each time a rat crossed all four paws into the arm, it was said to have entered the arm. Increased spontaneous alternations, or three successive arm entries, were considered as an indicator of improved learning and memory. The formula used to calculate the percentage of spontaneous alternations was [number of spontaneous alternations/ (total arm entries-2)] × 100.

6.2.4.8.6 Neurochemical analysis

Animals from each group were immediately sacrificed by cervical dislocation following the Y-maze test, and their hippocampal brain section was isolated. The tissue samples were

centrifuged at 4 °C at 15000 *g* for 20 min after that 10 mM phosphate-buffered saline pH 7.4 was added. By using the Bradford assay, the protein content of the supernatant was calculated.

6.2.4.8.7 *In-vivo* AChE estimation

AChE was estimated in the brain of the animal by Ellman's method [142, 143]. 100 µL of the supernatant was incubated with 15 mM of freshly prepared ATCI (100µL) in presence of 2.7 ml of phosphate buffer for 5 min. With a Multimode Microplate Reader (BioTek Synergy, USA), the rate of increase in absorbance was measured spectrophotometrically at 415 nM after addition of 100 µL of 1.5 mM DTNB. The rate of hydrolysis was calculated as µM of substrate hydrolyzed/min/mg of protein.

6.2.4.8.8 ACh level determination:

Following the manufacturer's instructions, the enzyme-linked immunosorbent assay (ELISA) kit was used to determine the level of Ach in the cortex. The standard calibration curve was used to calculate the Ach concentration.

6.2.4.9 Aβ1-42 induced ICV rat model: Morris water maze test.

Fresh groups of adult male Wistar rats weighing 200–250 g underwent the ICV rat model. The four groups of six rats each included the sham (control), model ($A\beta_{1-42}$), donepezil (5 mg/kg, *p.o.*), and compound **72** (20 mg/kg, *p.o.*) groups of rats. The $A\beta_{1-42}$ (Sigma Aldrich, India) was dissolved in sterile saline (0.9% NaCl) solution. Briefly, rats were individually mounted on stereotaxic equipment after being anaesthetized using ketamine (100 mg/kg, i.p.) and xylazine (10 mg/kg, i.p.). The scalps of rats were washed with iodine solution and saline after the ear bars were symmetrically placed. The stereotaxic coordinates corresponding to the bregma were set (-0.5 mm anteroposterior, +1.2 mm mediolateral, -3.2 mm dorsoventral with incision bar set at -3.3mm), and a hole was drilled through the skull.

With the exception of the sham group, all of the rats received an injection of $A\beta_{1-42}$ (5 µl, 4 µM) using a Hamilton microsyringe at a 2 µl/min infusion rate. The needle was left in place after

injection for an additional five minutes to stop reflux. In place of $A\beta_{1-42}$, the rats in the sham group simply received vehicle. All the rats were given special care after surgery, and iodine ointment was frequently administered to the surgical site until spontaneous feeding returned. Following a seven-day period of post-operative recuperation, donepezil and compound **72** were orally administered to the corresponding group of animals starting on the eighth day and continuing through the sixteenth day. During the final four days of therapy (13–16 days), the Morris water maze experiment was carried out to evaluate learning and memory. In order to assess the escape latency time and the number of platform crossings during a period of 90s, two trials per day were performed at an interatrial difference of 3 h. The water maze device was a circular pool with dimensions of 121 cm in diameter, 62 cm in height, and 32 cm in depth. TiO2 was used to make the pool opaque after it had been filled with water (25±2 °C). The pool was divided into four equal quadrants, one of which had a hidden platform that was 2 cm under the surface of the water. To measure the escape latency time (the amount of time needed to reach the hidden platform) and the number of platform crossings during the course of 90s, the experiment was carried out on all of the rats for five days in a row. In a soundproof room, all readings were photographed with the use of a camera.

6.2.4.9.1 BACE1 activity assay

20 mg of tissue were homogenised in 500 µL of lysis buffer containing 150 mM NaCl, 1% Triton X-100, and 0.1% protease inhibitor cocktail in order to assess the BACE1 activity in the tissues of the hippocampal region. The homogenates were centrifuged at 10,000g for 10 min at 4 °C, and the supernatants were collected to calculate the protein content using the Bradford method. Using a commercial BACE1 fluorescence resonance energy transfer kit (Sigma Aldrich, India, Catalogue Number CS0010) in accordance with the manufacturer's instructions, the BACE1 activity was assessed using 300 µg of protein from the homogenised samples. Fluorescence units are used to express BACE1 activity.[144].

6.2.4.9.2 DCFH-DA study for estimation of ROS levels

The dichloro-dihydro-fluorescein diacetate (DCFH-DA) production oxidation assay was used to measure the 2′-7′-dichloroflurescein diacetate (DCFH-DA) levels as a measure of the peroxide production in the cellular components. According to Halliwell and Gutteridge (2005), this experimental method of analysis is based on the deacetylation of the DCFH-DA probe and its subsequent oxidation into DCF, a highly fluorescent compound, by reactive species. The DCFH-DA method was used to calculate the ROS levels in brain homogenate. The brain homogenate's supernatant was added to a medium containing 10 mM of Tris-HCl buffer (pH 7.4). A microplate reader (BioTek, USA) was used to measure the amount of DCF fluorescence. The fluorescence intensity (at 522 nm) was inversely correlated with the levels of mitochondrial ROS[145].

6.2.5 Molecular dynamics & simulation

Molecular dynamics simulations are essential in studying drug-protein docking interactions, providing detailed insights into the dynamic behavior of molecules over time. It helps to validate and refine docking predictions by comparing predicted binding modes with actual dynamic behavior, identifying false positives and improving computational accuracy. MD simulations provide a dynamic representation of the interaction between a drug and its target protein, allowing us to observe how the protein and ligand evolve over time. They can capture conformational changes in both the protein and ligand during the binding process, particularly for targets that undergo significant structural rearrangements upon ligand binding. MD simulations can reveal potential unstable configurations or transient states of the complex, which is crucial for understanding the dynamics of the interaction and predicting potential dissociation pathways. Predicting possible dissociation pathways and comprehending the dynamics of the interaction depend heavily on this information. MD simulations can shed light on the long-term stability of drug-protein complexes, particularly when they are run for longer

periods of time. This is crucial to comprehending how long-lasting the binding relationship is in physiological settings.

The system was subjected to molecular dynamic simulation for 50 ns run in the NPT ensemble (T = 310.15 K) at a constant pressure of 1.01 bar. The trajectory coordinate and energy of the system was recorded at 1.2 ns. The protein ligand complex of compound **72** was subjected to MD simulation. The Protein Preparation Wizard of Maestro Academic Visualizer version 11.5.01 was used to optimize the PDB file. The bond order, hydrogens were assigned and incorrect bonds were corrected. An orthorhombic water box with a 10 buffer gap between the walls of the box and the protein atoms was defined as the global. Additionally, the salt concentrations were adjusted to 0.15 M by neutralizing the system with Na+ ions. The default OPLS force field was applied to this system, and energy minimizations were carried out using a convergence gradient of 1 Kcal/mole for a maximum of 2000 iterations.

Molecular dynamic simulations for this system were performed for 50 ns in the NPT ensemble (T = 310.15 K) with a constant pressure of 1.01.

The molecular dynamics simulation was run using the "Academic version of Desmond" (Desmond 2020-3) to study the change in protein structure within the solvent system. Desmond's System Builder panel was used to design the water-soaked solvated system. For the simulations, the complex was centered in an orthorhombic cubic box with periodic boundary conditions and filled with single-point charge (SPC) water molecules buffered at a distance of a minimum of 10 Å between a protein atom and box edges. The system was neutralized by adding counter-ions (Na+ and Cl-) at random, and an isosmotic state was maintained by adding 0.15 M NaCl. Using OPLS 2005 force field parameters as the default protocol associated with Desmond, the solvated built system was minimized and relaxed. MD simulations were performed using an isothermal, isobaric ensemble (NPT) with a temperature of 300 K, pressure of 1 atm and a 200 ps thermostat relaxation period. A total of 100 ns

simulations were run, during which 1000 trajectories were recorded. Finally, the Simulation Interaction Diagram (SID) tool was used to examine the MD simulation trajectory. The interaction energies between the protein and the ligand poses were computed using the MM-GBSA (molecular merchandised generalized-born/surface area) method implemented by Schrodinger. The average post dynamic binding free energy (ΔG bind) based on MM-GBSA was calculated using the thermal_mmgbsa.py script.

6.3 Results & discussions

6.3.1 Pharmacophore development and virtual screening

Pharmacophoric features *viz*. ring aromatic (A1 and A2), hydrophobic (HY), hydrogen-bond acceptor (HA), hydrogen-bond donor (HD) of co-crystalized ligand, ifenprodil (PDB ID: 3KMY) were identified. Shape based pharmacophore screening was performed on ZINC ligand database of 12,996,897 molecules. RMSD was set to 0.5 and the resultant search ligands were subjected to drug-likeliness and PAINS filters.

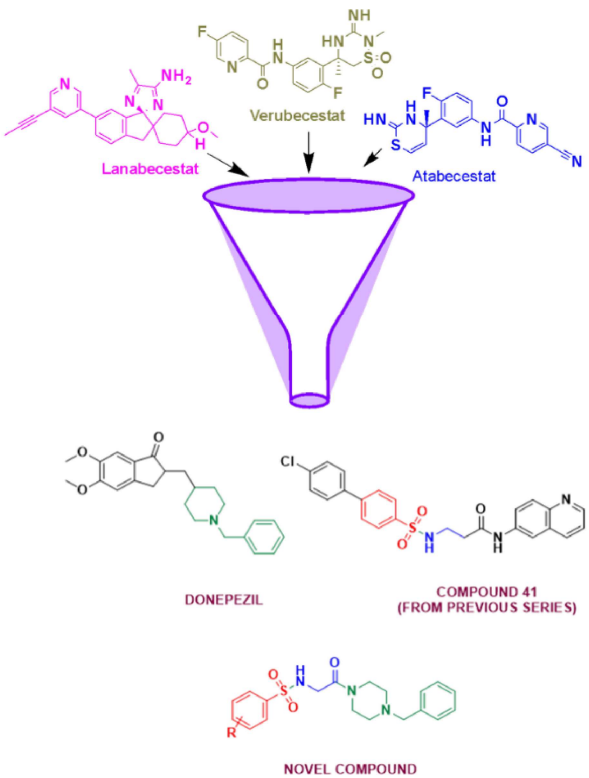

Figure 6.1 Design strategy for the multitargeted compounds.

6.3.2 Molecular docking

The molecular docking and dynamics simulation studies were performed to affirm the binding characteristics of designed ligands on AChE and BACE1. The binding energy of compound **72** with AChE (PDB ID: 4EY7) was found to be -11.93. The docking study of compound **72** showed π- π interaction with the peripheral anionic site residues Trp286, esteratic locus His447, as well as other residues such as Tyr337, Phe338.

A hydrogen bond was also visible between Try124 and the amide's carbonyl group. The residues Val 294, Phe 295, Arg 296 and Tyr 72 were on either side of the groove where the biphenyl group was positioned. Compound **72** also exhibited interactions with the ω-loop, including pi-alkyl interactions with Leu289 and Val294 and hydrogen bonds with Phe295 as shown in **Figure 6.2**

Co-crystallized ligands were initially docked into the corresponding grids of AChE and BACE1 to validate the docking parameters and prepared grids. The superposition tool was used to show RMSD values within 2 between co-crystallized and re-docked ligands in order to confirm the suitability of the generated grids and docking protocols.

The results of docking studies confirmed that designed ligands (65 through 64) and particularly the lead compound 72 accommodated within the active pocket of AChE with substituted phenyl group occupied PAS, while benzylpiperazine nucleus was extended deep into CAS and formed polar interactions with Ser203 and His447. The binding mode of docked ligands on BACE1 indicated significant interactions with both the catalytic aspartate residues (Asp32 and Asp228) through either ionic salt bridge or Hydrogen bonding. The binding energies as well as efficiencies of the series are summarized in the table (**Table 6.1**).

The compound **72** also showed decent ADME profile in *in silico* predictions with *in vitro* Caco-2 cell permeability (Human colorectal carcinoma) value at 21.2083 nm/sec, *in vitro* MDCK

cell permeability at 0.085 nm/sec and Percentage predicted human intestinal absorption Percentage predicted human intestinal absorption (HIA, %) at 96.73 which was carried out using PreADMET server and was found to be within acceptable reference limits.

Table 6.1 Binding energies of the compounds docked against AChE

Comp ID	Binding energy (Kcal/mole)	Binding efficiency
65	-8.91	-0.318
66	-9.26	-0.331
67	-8.21	-0.304
68	-9.7	-0.32
69	-10.18	-0.302
70	-8.76	-0.322
71	-10.88	-0.307
72	-11.93	-0.325
73	-10.46	-0.311
74	-9.5	-0.323
75	-8.96	-0.32
76	-8.63	-0.337
77	-9.16	-0.358
78	-12.25	-0.304
79	-8.95	-0.315
80	-8.88	-0.288
81	-9.86	-0.29
82	-8.35	-0.298
83	-11.11	-0.37
84	-9.23	-0.308
DNP	-12.41	-0.322

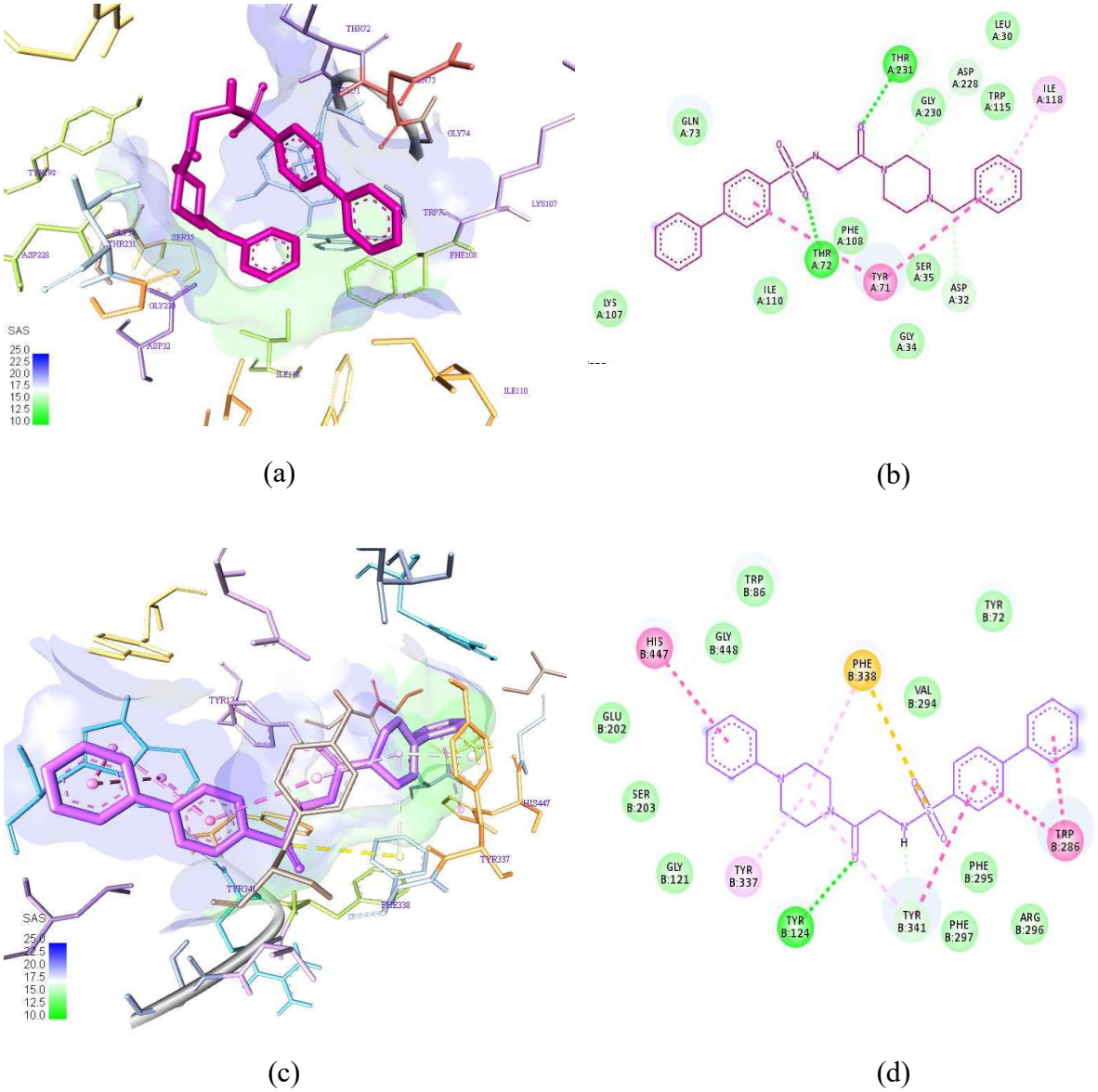

(a) (b)

(c) (d)

Figure 6.2 Docking poses of compound **72** against (a) AChE (PDB ID: 4EY7), (b) 2D representation of A, (c) BACE-1 (PDB ID: 3KMY), (d) 2D representation of C. The green dotted lines indicate conventional hydrogen bonds while the pink dotted lines indicate pi-pi interactions, similarly the pale pink dotted lines indicate Alkyl and Pi-alkyl interactions.

Table 6.2 Binding energies of the compounds docked against BACE1

Comp ID	Binding energy (Kcal/mole)	Binding efficiency
65	-8.91	-0.318
66	-9.26	-0.331
67	-8.21	-0.304
68	-8.91	-0.32
69	-9.26	-0.302
70	-8.21	-0.322
71	-8.63	-0.307
72	-9.36	-0.325
73	-9.33	-0.311
74	-8.89	-0.323
75	-8.46	-0.32
76	-8.4	-0.337
77	-8.71	-0.358
78	-10.25	-0.304
79	-9.78	-0.315
80	-10.37	-0.288
81	-8.51	-0.29
82	-8.82	-0.298
83	-8.65	-0.37
84	-8.71	-0.308
DNP	-12.41	-0.322

6.3.3 Chemistry

Compounds **30** to **44** were prepared by reacting substituted aromatic sulfonyl chlorides with the amino acid glycine. First step of the synthesis protocol was carried out in a mixture of water and acetone with sodium bicarbonate acting as the base. The compounds were characterized

by ^{1}H, ^{13}C NMR spectroscopy and Mass spectrometry. The acidic groups in the compounds were further reacted with various piperazines to yield compounds **65** to **84** as seen in **Table 6.3**

Table 6.3 Physico-chemical properties of the synthesized compounds

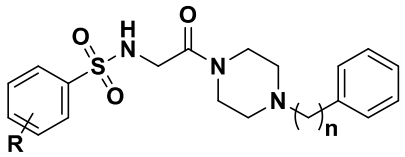

Comp.	R	n	R_f	% yield	M.P. (°C)
65	H	1	0.41	75	189-191
66	4-Cl	1	0.50	76	182-184
67	4-Br	1	0.49	83	181-183
68	4-NO_2	1	0.48	78	192-194
69	2- NO_2	1	0.51	80	183-185
70	4-OMe	1	0.53	75	185-187
71	4-CN	1	0.65	81	172-174
72	4-Phe	1	0.65	89	189-191
73	Naphthyl	1	0.70	84	194-196
74	4-(sec butyl)	1	0.71	78	204-206
75	4-H	1	0.61	77	235-237
76	4-Cl	2	0.63	76	240-242
77	4-Br	2	0.57	78	207-209
78	4-Phe	2	0.60	79	201-203
79	2-NO_2	2	0.62	71	280-281
80	4-NO_2	2	0.57	78	217-219
81	4-CN	2	0.56	79	216-218
82	4-OMe	2	0.58	84	189-191
83	4-(sec butyl)	2	0.45	77	213-215
84	4-Napthyl	2	0.62	75	201-203

6.3.4 Biological Evaluation

6.3.4.1 In-vitro AChE and BChE enzyme inhibition assays

Donepezil (DNP) and Rivastigmine (RVS) were used as positive reference standards. The inhibitory potential of the synthesised compounds **65**–**84** against AChE and BChE was determined by Ellman method and the results are presented in **Table 6.4**. With the exception of compound **76** ($IC_{50} > 50$ μM), the results demonstrated moderate to excellent inhibition of AChE in the micromolar to submicromolar concentration range. All of the compounds tested demonstrated a good to moderate BChE inhibitory potential. The para unsubstituted compounds **65** and **75** exhibited excellent AChE inhibition, with compound **65** showing an IC_{50} of 30.92 ± 2.47 μM, while compound **75** displayed nanomolar range activity at an IC_{50} of 0.053±0.003 μM. In comparison to the 53.55-fold selectivity of donepezil, (DNP: $IC_{50} = 0.018 \pm 0.001$ μM (AChE); $IC_{50} = 0.964 \pm 0.067$ μM (BChE)), compound **72** (a para phenyl derivative) from the series demonstrated 91.30-fold AChE selective inhibition (72: $IC_{50} = 0.046 \pm 0.003$ μM (AChE); $IC_{50} = 4.202 \pm 0.215$ μM (BChE)), while the selectivity index for Rivastigmine (RVS: $IC_{50} = 0.093 \pm 0.006$ μM (AChE), $IC_{50} = 0.035 \pm 0.002$ μM (BChE)) was found to be 0.376. Compound **73** (a para napthyl derivative) also showed decent activity with a selectivity index of 148.097 (73: $IC_{50} = 0.062 \pm 0.004$ (AChE); $IC_{50} = 9.162 \pm 0.831$ μM (BChE)). Among all the evaluated compounds, the AChE inhibitory activity of the compounds having electron donating groups at the para position (**70, 72, 74,78, 82,** and **83**) was considerably more prominent than that of the compounds having electron withdrawing groups (**66-69, 71, 76, 77, 79,** and **80**) at their para/ortho positions.

6.3.4.2 In-vitro BACE1 enzyme inhibition assay

FRET-based BACE1 fluorescence assay kit (Sigma Aldrich, Catalogue No. CS0010) was used to assess all the synthesized derivatives for their ability to inhibit BACE1. The results of the assay are presented in the **Table 6.4.** The BACE1 activity of the unsubstituted derivatives **65**

was not very potent (**65:** IC_{50}>200 μM) while compound **75** was found to moderately inhibit the enzyme (**75**: IC_{50}=107.26 ± 8.265 μM). However, the BACE1 inhibitory potential was significantly improved in compounds with electron-donating groups (or electron releasing groups) i.e., **70, 72, 74,78, 82,** and **83**. Compound **72** showed the highest potency against BACE-1 (**72**: IC_{50}=0.44±0.071 μM) among all the electron donating group compounds. This activity coincides with the docking results which predicted pronounced binding energy for this compound. Presence of the phenyl substituent at the para position along with the piperazinyl linker length of n=1 seems to have positive effect of the inhibitory potential. An exception to this was compound **78,** which showed rather weak inhibitory activity against the enzyme indicated that the change in piperazinyl linker length to n=2 might have a detrimental effect on the inhibition potential although docking results showed decent binding. The inhibition potential of the electron withdrawing group substitutions (**66-69, 71, 76, 77, 79,** and **80**) was marginally different, with a few compounds being almost inactive against the enzyme (**66, 69,** and **79**). Two of the compounds (**69** and **79**) had nitro group at their ortho positions. These results suggested that substitutions of electron-withdrawing groups at para position rather than ortho position were preferred. Compounds **67** and **77** showed the highest potency (**67:** IC_{50} = 12.95±0.781 μM and **77:** IC_{50} = 3.82±0.193 μM) among the electron withdrawing group substituted compounds, both had bromo group at their para positions. Compound **73** showed the highest potency overall (**73:** IC_{50} = 0.26±0.781μM) in the entire series indicating that the napthyl group substitution at the para position is beneficial to the activity against BACE1.

Table 6.4 Structures and enzyme inhibition activities of the synthesized compounds

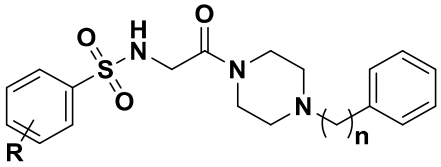

Comp.	R	n	IC_{50} (µM)			S. Ratio
			BACE 1	AChE	BChE	
65	4-H	1	>200	30.92± 2.47	***	***
66	4-Cl	1	>200	10.54±0.868	***	***
67	4-Br	1	12.95±0.781	37.809±2.562	***	***
68	4-NO_2	1	18.05±0.834	8.062±0.763	***	***
69	2- NO_2	1	>200	43.364±4.022	95.821±8.92	2.209
70	4-OMe	1	6.45±0.103	5.274±0.451	78.532±6.94	14.890
71	4-CN	1	15.30±0.963	19.21±1.502	***	***
72	4-Phe	1	0.44±0.071	0.046±0.003	4.202±0.215	91.30
73	Naphthyl	1	0.26±0.018	0.062±0.004	9.162±0.831	148.097
74	4-(sec butyl)	1	56.13±3.963	1.595±0.092	65.856±3.933	41.289
75	4-H	1	107.26±8.265	0.053±0.003	16.471±1.156	310.774
76	4-Cl	2	98.81±4.782	***	62.026±4.382	***
77	4-Br	2	3.82±0.193	0.633±0.042	***	***
78	4-Phe	2	***	1.052±0.086	***	***
79	2-NO_2	2	***	0.973±0.069	112.586±8.102	115.710
80	4-NO_2	2	26.81±1.742	15.869±1.251	76.521±4.947	4.822
81	4-CN	2	79.83±4.648	17.403±1.493	***	***
82	4-OMe	2	***	9.013±0.829	***	***
83	4-(sec butyl)	2	>200	7.921±0.064	36.024±2.681	4.548
84	4-Napthyl	2	>200	24.15±1.522	78.933±5.932	3.268
-	DNP	-	4.72±0.288	0.018±0.001	0.964±0.067	53.555
-	RVS	-	---	0.093±0.006	0.035±0.002	0.376

*** Inactive or showed less than 50% inhibitory activity at 50 µM concentration

6.3.4.3 Inhibition assay of metal induced Aβ1-42 aggregation and confocal fluorescence imaging

$A\beta_{1-42}$ upon incubation with the metal showed 100% aggregation. DNP, at a concentration of 20 µM produced significant inhibition of metal induced $A\beta_{1-42}$ aggregation and compound **72** was found to be more effective than DNP. It inhibited more than 50% of $A\beta_{1-42}$ aggregation, when compared with Fe^{+3}+ $A\beta_{1-42}$ and $A\beta_{1-42}$ groups (**Figure 6.3A**). Confocal imaging was performed to comprehend the interaction of $A\beta_{1-42}$, $FeCl_3$ and compound 72 at molecular level. Fluorescent background was obtained when dye ThT was used (**Figure 6.3B**). $A\beta_{1-42}$ aggregate was obtained when it was incubated and treated with ThT (**Figure 6.3C**) whereas, the fluorescence disappeared when $A\beta_{1-42}$ alone and $A\beta_{1-42}$ was incubated with the metal devoid of ThT. These blank images ascertained that neither $A\beta_{1-42}$ and metal nor their combinations showed any background noises in the absence of ThT. $A\beta_{1-42}$ incubated with metal showed aggressive plaque deposition (**Figure 6.3D**) while the plaques were disaggregated on treatment with compound **72**.

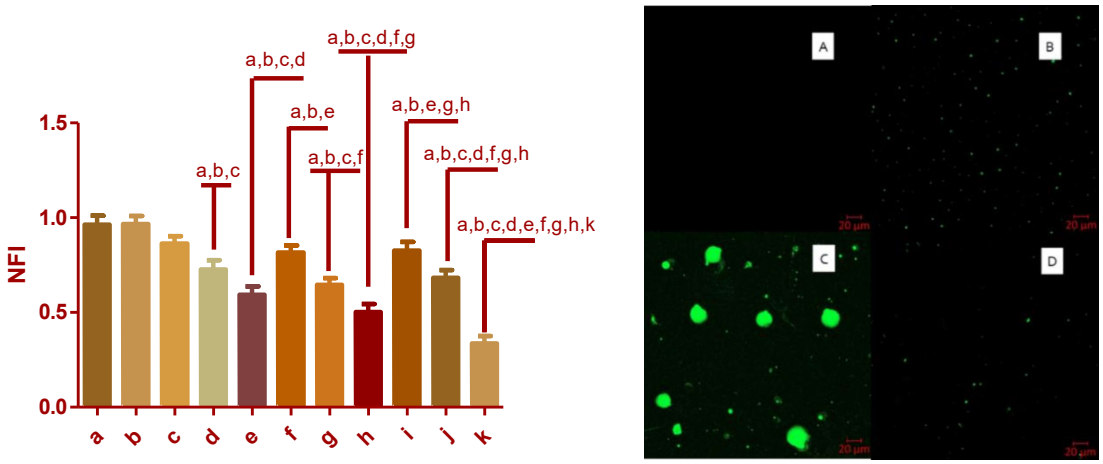

Figure 6.3 Inhibition assay of metal induced $A\beta_{1-42}$ aggregation assay and its confocal imaging (One-way ANOVA followed by Newman-Keuls multiple comparison test. $p < 0.05$ is considered as significant.), error bars represent the standard deviation (SD)

6.3.4.4 Neurotoxicity assay

Compound 72 was tested at concentrations of 15, 30, and 60 µM against donepezil at 20 µM (Figure 3). According to the results of the MTT assay, there was no discernible difference between the viability of the differentiated neuroblastoma cells at 30 µM maximum concentration and donepezil ($p < 0.05$). The cellular morphology remained unchanged at all of the selected concentrations. As a result, it can be said Compound 72 was not neurotoxic and can be taken up for additional preclinical studies. The Mean ± standard deviation (SD) of three independent experiments (n = 3) were used to illustrate the results as seen in **Figure 6.4.**

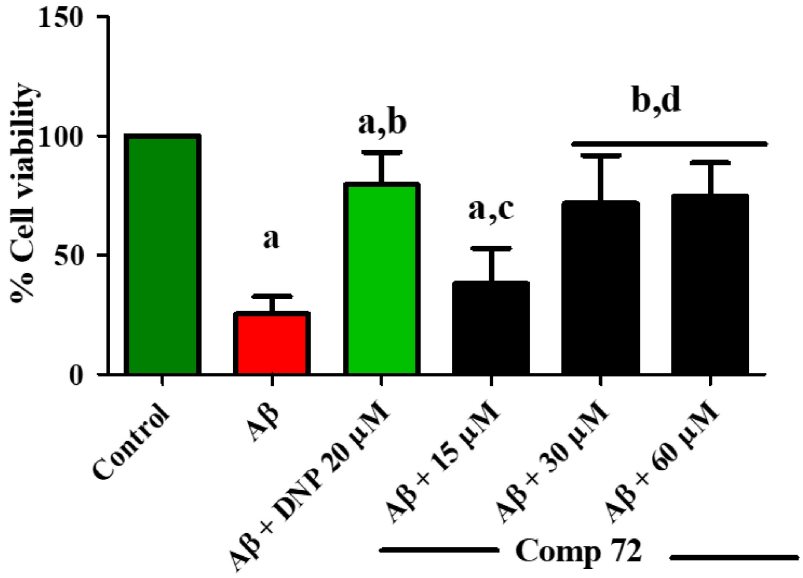

Figure 6.4 Cytotoxicity assay of compound **72** (15, 30 and 60 µM) on MC 65 cell line (One-way ANOVA followed by Newman-Keuls multiple comparison test. $p < 0.05$ is considered as significant.), error bars represent the standard deviation (SD) .

6.3.4.5 Neuroprotection assay

AD has been linked to neuronal death, and among other factors , ROS are believed to be primarily responsible. In the absence of tetracycline (TC-), the mutant neuronal cell line MC65 generates Aβ, which causes the production of ROS. At doses of 50 and 100 µM, compound **72**

significantly reduced the amount of Aβ produced as compared to TC- cells as seen in **Figure 6.5**

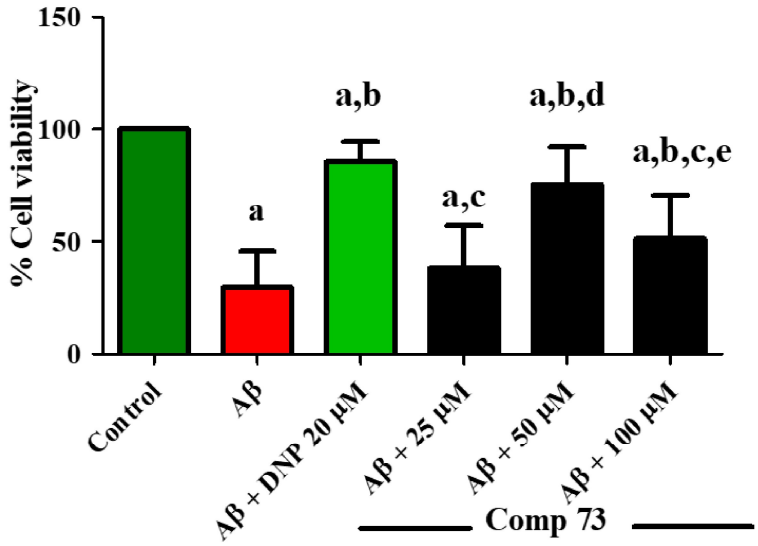

Figure 6.5 Neuroprotection assay of compound **72** (25, 50 and 100 µM) on MC 65 cell line (One-way ANOVA followed by Newman-Keuls multiple comparison test. $p < 0.05$ is considered as significant.), error bars represent the standard deviation (SD).

6.3.5 In-vitro blood-brain barrier permeation assay (PAMPA)

The main requirement for AD drugs is permeation through the blood-brain barrier. The parallel artificial membrane permeation assay (PAMPA) was used to screen all the synthesised derivatives for BBB permeation. BBB permeability (Pe) of nine commercially available drugs was assessed as a benchmark. **Table 6.5** contains the Pe values of the compounds (**65-84**). Alkyl linker derivative (compound **75**; $Pe = 6.925 \pm 0.012 \times 10^{-6}$ cm s^{-1}), demonstrated better BBB permeability, out of all the derivatives, which was likely due to the longer linker chain. The single carbon linker compounds (**66**; $Pe = 6.491 \pm 0.34 \times 10^{-6}$ cm s^{-1} and **70**; $Pe = 6.694 \pm 0.05 \times 10^{-6}$ cm s^{-1}) also showed appreciable BBB permeability. Additionally, all of the tested substances had good *in-vitro* permeation potentials and could cross the BBB.

Table 6.5 PAMPA-BBB assay of the synthesized compounds

Comp.	Pe (10-6 cm s-1)a,b	Permeability prediction (CNS+/-) d
65	5.655±0.04	CNS+
66	6.491±0.34	CNS+
67	5.513±0.23	CNS+
68	5.9905±0.01	CNS+
69	5.729±0.007	CNS+
70	6.694±0.05	CNS+
71	5.606±0.008	CNS+
72	6.627±0.009	CNS+
73	6.656±0.06	CNS+
74	6.748±0.004	CNS+
75	6.925±0.012	CNS+
76	6.964±0.04	CNS+
77	6.748±0.003	CNS+
78	5.367±0.03	CNS+
79	5.369±0.017	CNS+
80	5.664±0.02	CNS+
81	6.731±0.004	CNS+
82	6.627±0.009	CNS+
83	6.76±0.05	CNS+
84	6.529±0.017	CNS+
CPZ	6.20 ± 0.30	CNS+

6.3.6 Propidium iodide displacement assay

Propidium iodide is replaced by inhibitors when they bind to PAS, causing the intensity of the fluorescence to diminish. Compounds **72** and **73** demonstrated greater displacement of propidium iodide (**72**: 10 mM= 15.68 %, 50 mM= 28.04%; **73**: 10 mM = 21.24%, 50 mM = 41.10%) compared to donepezil (10 mM= 21.30%; 50 mM=38.23%). Compounds **72** and **73** were selected for further stuies due to their balance of inhibitory potential against both targets

(AChE and BACE-1), as well as their very high displacement of propidium iodide from PAS-AChE. A PI assay was conducted to investigate the ability of compounds to displace PI from PAS-AChE at 10 μM and 50 μM.). Data are expressed in **Table 6.6** as the mean ± SEM of three separate experiments (n = 3).

Table 6.6 Propidium iodide displacement assay

Comp.	Displacement of PI from AChE PAS (% inhibition)	
	Conc. 10 μM	**Conc. 50 μM**
72	15.68 ± 1.96	28.04 ± 2.81
73	21.24 ± 2.18	41.10 ± 2.49
DNP	21.30 ± 1.69	38.23 ± 3.37

6.3.7 Scopolamine induced amnesia model

6.3.7.1 Y maze test

On the seventh day of the trial, the Y-maze test was conducted to assess the effect of the test compound 72, and spontaneous alternations were calculated as a test of spatial working memory. In the scopolamine group of animals, the percentage spontaneous alternations were significantly lower than in the control group (**Figure 6.6**, $^{a}p < 0.05$), suggesting that memory and learning impairment had been induced. When compared to scopolamine, donepezil (5 mg/kg) significantly increased spontaneous alternations (**Figure 6.6**, $^{d}p < 0.05$). The fact that the total arm entries of all the groups remained constant demonstrates that scopolamine did not impair locomotor activity. Overall, the scopolamine-induced model using Y maze test supported the potential of compound **72** to enhance spatial and short-term memory.

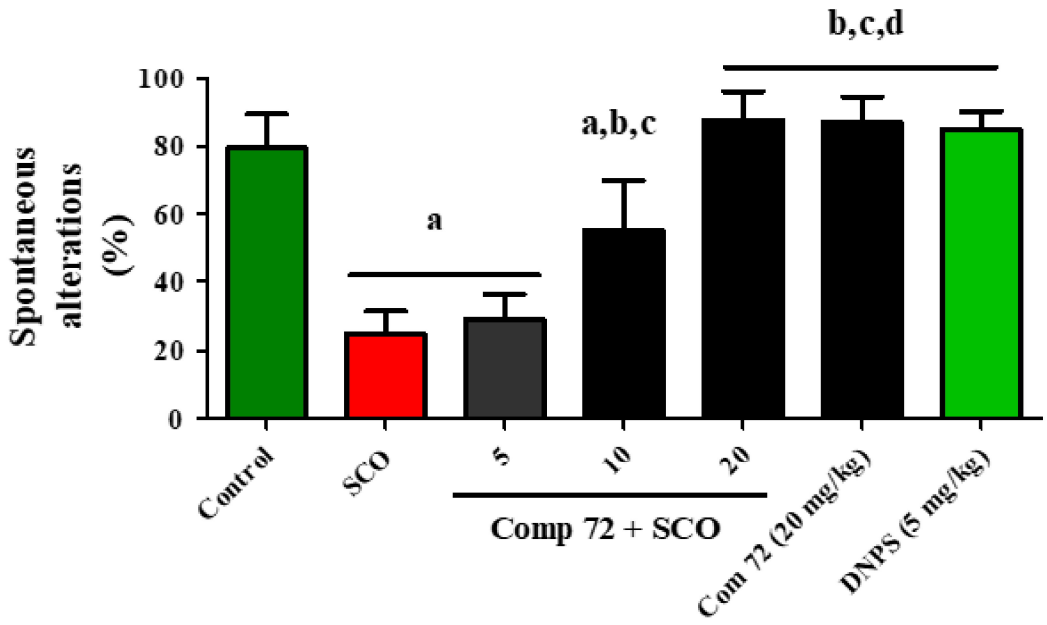

Figure 6.6 Effect of compound **72** on scopolamine-induced impairment of spontaneous alternation behaviour score (spontaneous alternation %); data are expressed as mean ± SEM (n = 6): $^{a}p < 0.05$ compared to vehicle control; $^{b}p < 0.05$ compared to SCO, $^{c}p < 0.05$ compared to 5 mg/kg, $^{d}p < 0.05$ compared to test compound at 10 mg/kg [One way ANOVA followed by Newman-Keuls multiple comparison test. $p < 0.05$ is considered as significant] , error bars represent the standard deviation (SD).

6.3.7.2 *In-vivo* AChE estimation

Ellman colorimetric assay was used to estimate the AChE activity. The findings showed that the AChE activity in the scopolamine-group of samples was significantly higher ($p< 0.05$,) than that in the healthy control group. In comparison to the scopolamine-group, the hippocampal homogenate samples from the groups treated with compound **72** significantly reduced the AChE activity ($p< 0.05$). Additionally, it was found that there was no difference in AChE activity between donepezil (5mg/kg) and compound **72** (20mg/kg), although the compound had slightly lower AChE inhibitory activity at 5mg/kg ($p<0.05$) than donepezil (**Figure 6.7**).

Overall findings showed that compound **72** effectively penetrated the BBB and significantly reduced AChE levels in the hippocampal brain.

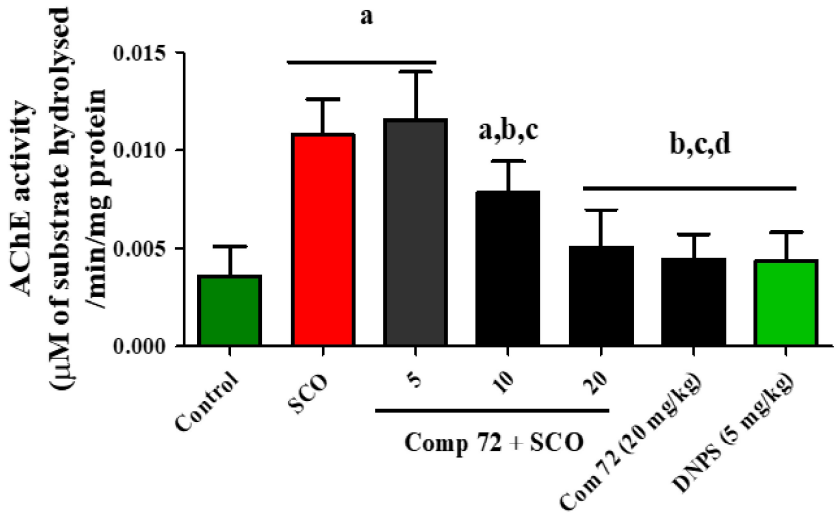

Figure 6.7 Estimation of AChE level (Mean ± SD, n = 6, [a]p < 0.05 compared to vehicle control; [b]p < 0.05 compared to SCO; [c]p < 0.05 compared to 5 mg/kg; [d]p < 0.05 compared to 10 mg/kg. (One-way ANOVA followed by Newman-Keuls multiple comparison test. p < 0.05 is considered as significant.), error bars represent the standard deviation (SD)

6.3.7.3 ACh neurotransmitter assay result

ACh is produced in cholinergic neurons and then is stored in the presynaptic membrane vesicles. The vesicles and presynaptic membrane fuse when the nerve impulse reaches the nerve ends, releasing ACh through exocytosis. The balancing action of AChE causes the released ACh to be subsequently hydrolyzed. Learning and memory impairment as well as cognitive dysfunction arise from lowered levels of ACh in the synaptic region. The ACh level was considerably lower in the SCO group, whereas the treatment groups had significantly higher Ach content at 10 and 20 mg/kg in a dose-dependent manner and were comparable to that of DNP at 5mg/kg (**Figure 6.8**).

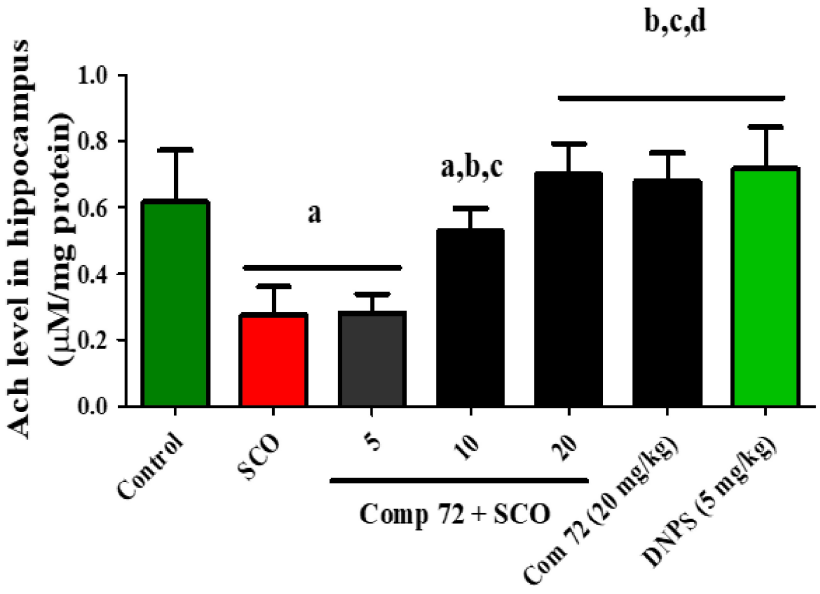

Figure 6.8 Elevation of ACh content in SCO rats. Sham-operated rats were used as controls, whereas SCO rats were untreated or treated with 5, 10 and 20 mg/kg of Compound 72 whereas DNP was given at 5 mg/kg. (One-way ANOVA followed by Newman-Keuls multiple comparison test. $p < 0.05$ is considered as significant.), error bars represent the standard deviation (SD)

6.3.7.4 Aβ1-42 induced ICV rat model: Morris water maze test.

One of the most promising ways to create learning and memory deficits coupled with the AD-like phenotypic condition is to administer $A\beta_{1-42}$ intracerebroventricularly (ICV). $A\beta_{1-42}$ is the main component of the senile plaques found in the brains of AD patients and enhanced activity of BACE1 has been shown to accelerate Aβ deposition. By injecting $A\beta_{1-42}$ intracranially (ICV) into the hippocampus region of healthy Wistar rats, the effect of the lead molecule **72** was evaluated.

With the exception of the sham group, all animal groups have received the ICV $A\beta_{1-42}$ injection. Rats from all groups received the appropriate treatments for nine consecutive days after a seven-day recovery period. The Morris water maze experiment was conducted to measure escape latency time (ELT) and the number of platform crossings over a 90-second period

during the final four days of treatment. As a result of $A\beta_{1-42}$ treatment, the ELT was considerably prolonged (**Figure 6.9**, $p < 0.05$), and the number of platform crossings (**Figure 6.9**, $p < 0.05$) gradually decreased in the model group of animals compared to the sham group, suggesting that learning and memory were impaired.

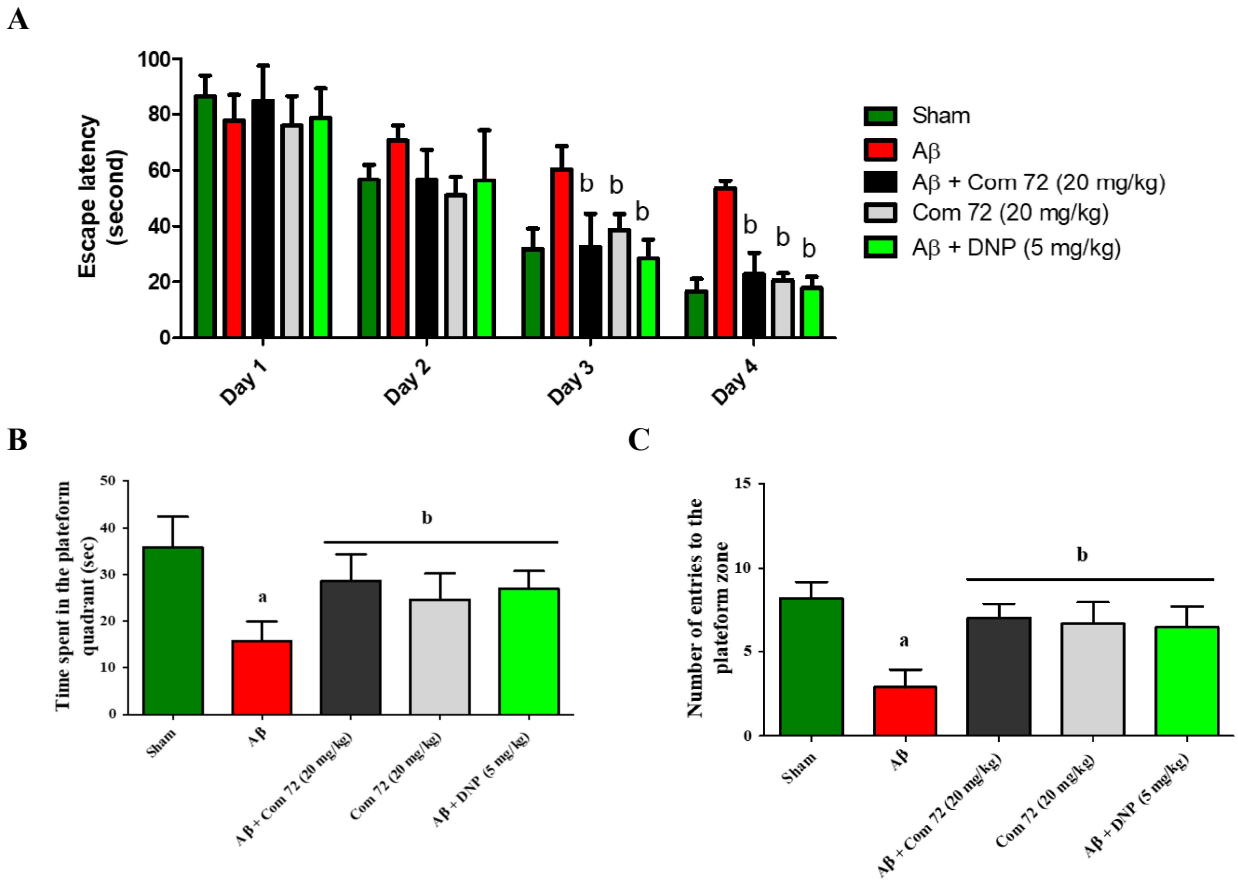

Figure 6.9 Protective effect of compound **72** on $A\beta_{1-42}$ induced memory deficits the Morris water maze test. (A) Escape latency during the training trials in the MWM tests; (B) Time spent in the platform quadrant; (C) The number of entries to platform zone during the probe trial; The data are presented as the mean ± SEM (n=6) with one-way ANOVA followed by Tukey test and two-way ANOVA followed by Bonferroni multiple comparison test. $^{a}p < 0.05$ compared to sham and $^{b}p < 0.05$ compared to $A\beta_{1-42}$.

6.3.8 BACE1 activity assay

The changes in the BACE1 activity in the rat hippocampus produced by the chronic administration of $A\beta_{1-42}$ were determined with a commercial kit (Sigma Aldrich, India, Catalog Number CS0010). Aβ group showed a statistically significant increase in BACE 1 activity compared with the sham group. However, there were no significant differences in the BACE1 activity levels among the $A\beta_{1-42}$ + Compound 72, Compound 72 alone and DNP groups as compared to the sham (**Figure 6.10)**.

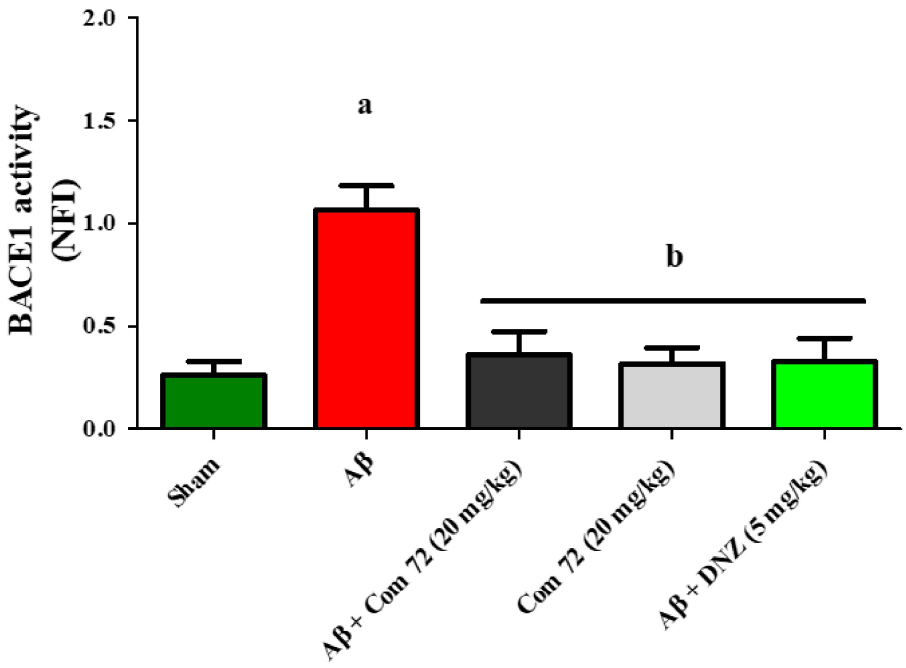

Figure 6.10 BACE-1 activity from the rat brain. (One-way ANOVA followed by Newman-Keuls multiple comparison test. $p < 0.05$ is considered as significant.), error bars represent the standard deviation (SD).

6.3.8.1 DCFH-DA study for estimation of ROS levels

ROS levels in the brains of animals treated with $A\beta_{1-42}$ were significantly higher than those in the sham group ($p < 0.05$). In the brains of sham group and treatment only group (Compound **72**), there was no significant difference in the levels of ROS. Additionally, ROS levels in the

brains of $A\beta_{1-42}$ group animals, treated with compound **72** were found to be comparable to those of the sham group animals and lower than those of the $A\beta_{1-42}$ group (**Figure 6.11,** $p < 0.05$).

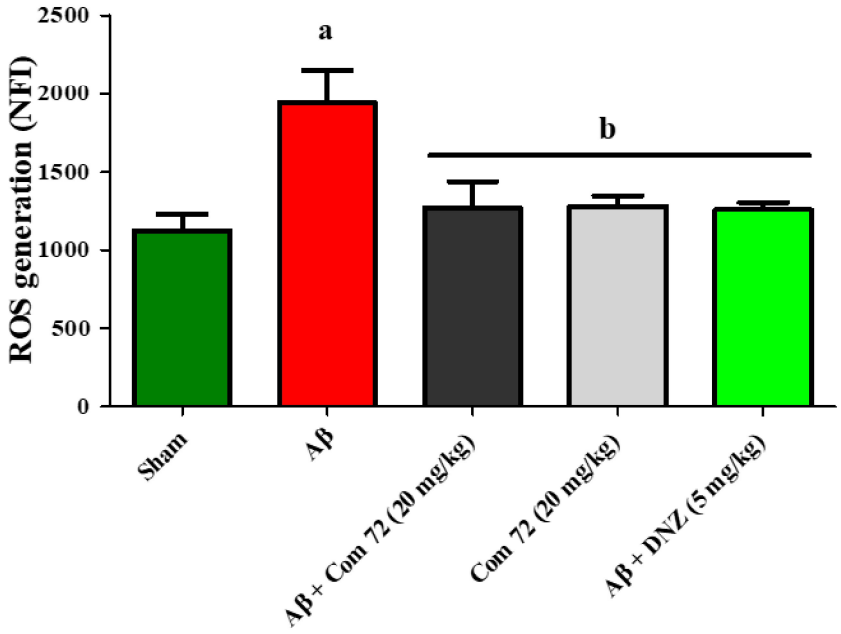

Figure 6.11 Oxidative stress as seen in animals experimentally induced with $A\beta_{1-42}$ according to reactive oxygen species (ROS) levels. (One-way ANOVA followed by Newman-Keuls multiple comparison test. $p < 0.05$ is considered as significant.), error bars represent the standard deviation (SD)

6.3.9 Molecular dynamics simulations

Molecular dynamics simulation of protein ligand complex of compound 72 was performed for 100 ns. It indicated that presence or absence of ligand in the active site of protein did not affect the global RMSD of protein. Further, the simulation of protein along with compound 72 also displayed a similar and highly consistent binding with an average RMSD of 1.84 Å, which was acceptable for proteins. The ligand RMSF of compound 72 revealed that groups 11 to 16 exhibited greater flexibility than other regions of molecule (**Figure 6.12**). It was also observed that compound 72 displayed hydrogen bond interactions with residues Phe 295 and Tyr 341 for more than 50 percent of total run time. The hydrophobic interactions were also significant in

contributing ligand-receptor stability through residues Tyr109, Phe133 and TYR239 for signification fraction of time. The compound also showed water mediated hydrogen bonding through residue Arg 296 (**Figure 6.13**).

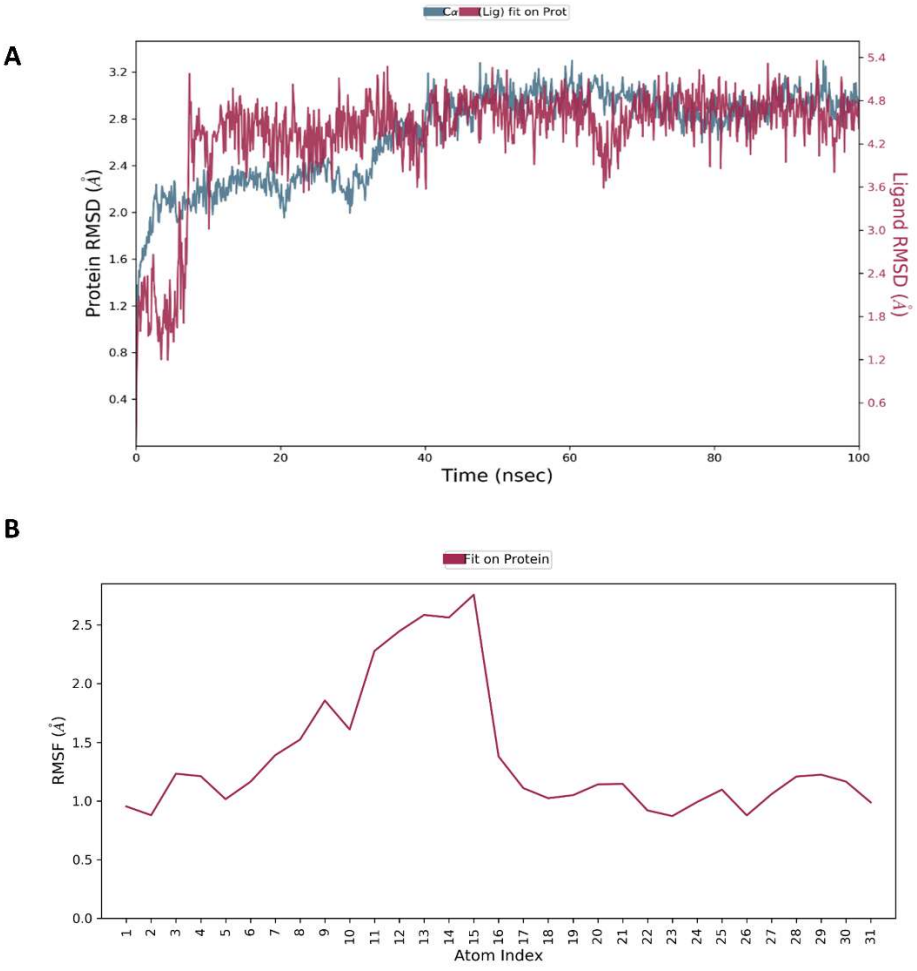

Figure 6.12 Results of the Molecular dynamics simulations studies conducted for the Compound **72** docked against the protein 4ey7 for 100ns. **A**. RMSD (Å) vs. time (100 ns); **B** RMSF (Å) vs. time (100 ns)

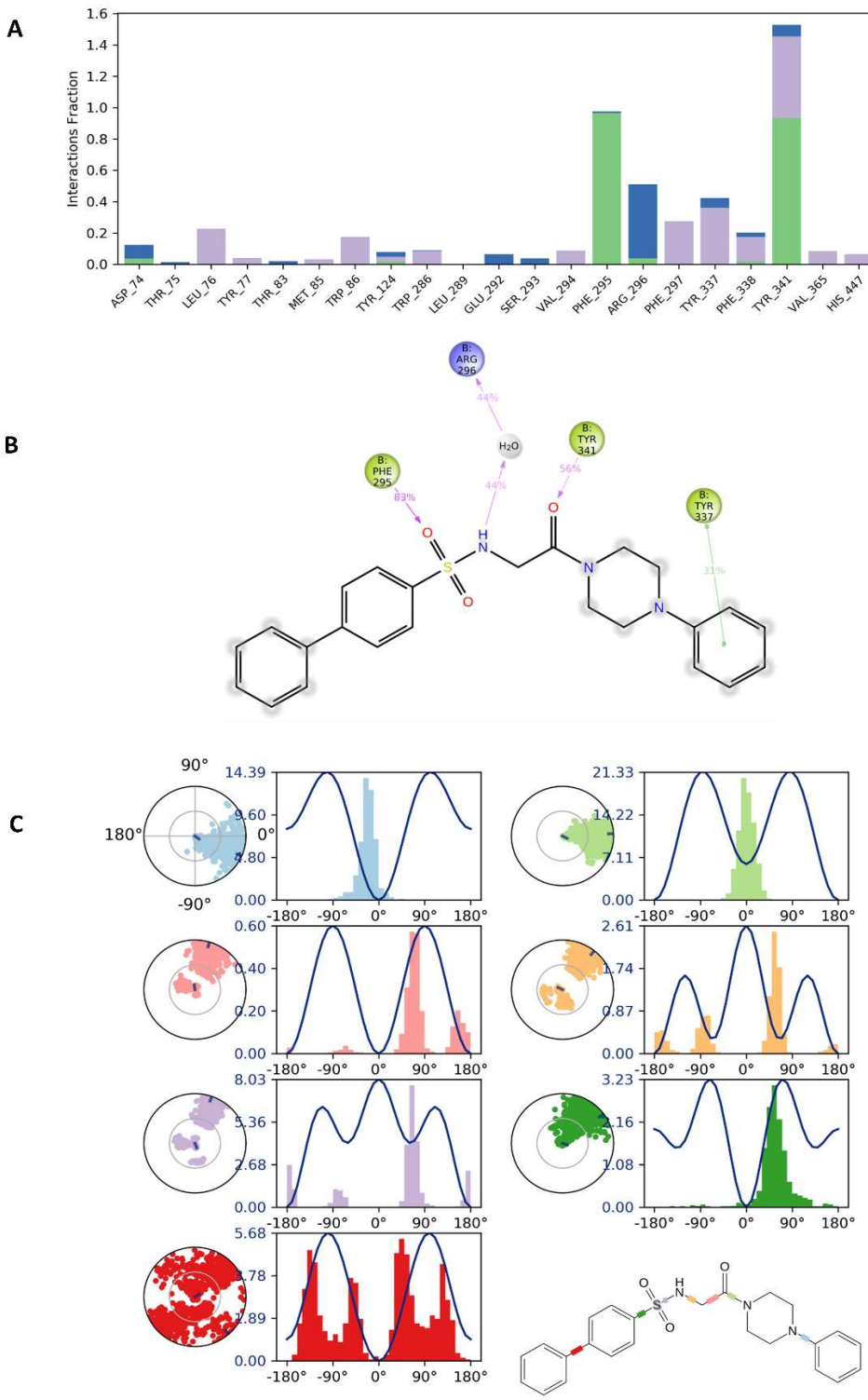

Figure 6.13 Results of the Molecular dynamics simulations studies conducted for the Compound **72** docked against the protein 4ey7 for 100ns. **A**. Interaction fractions; **B**. Ligand contacts; **C**. Torsion profile

6.4 Conclusions

AD is a multifactorial complex disorder, and its progression and development are influenced by a number of pathophysiological mechanisms. The progression of the disease is not contained by the current therapeutic regimens; only its symptoms are relieved. The development of effective drug candidates to treat AD has shown promise and is being investigated using a single molecule-multiple target approach. Using pharmacophore models and their co-crystallized ligands such as donepezil, it is made possible to identify the potential lead containing the N-benzylpiperazine nucleus as a multitarget-directed ligand against AChE and BACE1.

The compounds were designed by using the scaffold hopping guided MTDLs strategy through incorporation of the pharmacophoric features from the lead molecule (previous section) in addition to which the structural features essential for inhibition of the beta-site amyloid precursor protein cleaving enzyme 1 (BACE1) were added. In order to improve binding with AChE and BACE1, a series of N-benzylpiperazine analogues were rationally created through strategic modifcation of the earlier developed leads. The outcomes of studies using molecular docking and dynamics simulations were also supported by the results of designed ligands.

The designed series includes a library of twenty novel N-(2-oxo-2-(4-phenylpiperazinyl) ethyl) and N-(2-(4-benzylpiperazinyl)-2-oxoethyl) sulfonamide derivatives. The compounds were finalised after docking studies against all three targets (AChE, BACE1 and $A\beta_{1-42}$) and were then synthesized, purified & characterized. IC_{50} against BACE1, AChE & BChE was determined. Blood brain barrier (BBB) penetration was estimated using PAMPA assay. The Propidium iodide assay was carried out for establishing AChE specificity. Compound **72** was found to be the most potent followed by compound **73**. $A\beta_{1-42}$ aggregation inhibition assay followed by confocal imaging were performed. *N-(2-oxo-2-(4-phenylpiperazin-1-yl) ethyl)-[1,1'-biphenyl]-4-sulfonamide* (compound **72**) exhibited potent inhibitory activities against

hAChE (IC_{50} = 0.093 ± 0.01 µM, hBChE IC_{50} = 4.202±2.15 µM), BACE1 (IC_{50} = 0.44±0.071µM) as well as significant amyloid-beta aggregation (10 and 20 µM) inhibition. Compound **73**, N-(2-(4-benzylpiperazin-1-yl)-2-oxoethyl) naphthalene-2-sulfonamide with the benzyl linker in its structure, showed higher potency against BACE1 (IC_{50} = 0.26±0.1781 µM compared to Compound **72**, however, it was less potent against hAChE (IC_{50} = 0.062±0.004 µM, hBChE 9.162±8.31µM). The compounds showed optimal blood-brain barrier permeability (compound **72**, *Pe* = 6.627±0.009 x 10^{-6} cm s^{-1}, compound **73**, *Pe* = 6.656±0.06 x 10^{-6} cm s^{-1} in PAMPA assay and displayed neuro protective properties (40 µM) on SH-SY5Y neuroblastoma cell lines. Compound 72 also showed stable interactions with the protein 4ey7 (AChE) throughout the 100 ns of molecular dynamics simulations carried out in the NPT ensemble (T = 310.15 K) at a constant pressure of 1.01 bar. with an average RMSD of 1.84 Å.

Propidium iodide was successfully displaced from PAS-AChE by compound 72, and Aβ aggregation was inhibited. Confocal fluorescence microscopy studies were used to characterise the morphology of the Aβ aggregates. Compound 72 was found to be free of neurotoxicity towards SH-SY5Y neuroblastoma cell lines even at the highest tested concentration of 60 µM. In a dose-dependent manner, the Y-maze experiment assessed the effects of compound 72 on scopolamine-induced cognitive dysfunction. The constant total number of arm entries across all groups demonstrates that scopolamine had no detrimental effects on the animals' ability to move. The scopolamine-induced model supported compound 72's capacity to enhance spatial and short-term memory. Through the use of the DCFHDA studies, ex vivo and biochemical analysis of the evaluated compounds demonstrated a significant inhibition of the brain AChE as well as a favourable change in the biomarkers of oxidative stress. On the final five days of treatment, the Morris water maze experiment was used to measure escape latency time (ELT) and the number of platform crossings over a 90-second period. Learning and memory were compromised, as evidenced by the prolonged ELT following treatment with $A\beta_{1-42}$ and the

gradually declining number of platform crossings in the model group of animals compared to the sham group. Results from *in vivo* tests confirmed those from computational and *in vitro* research. The majority of the evidence points to compound 72 as the most promising multi-target directed ligand and possible "lead" in the fight against AD.